 doi:10.20944/preprints202206.0289.v1

Article

Flat Slabs in Eccentric Punching Shear: Experimental Database and Code Analysis

Daniel Vargas [1*], Eva O. L. Lantsoght [1, 2] and Aikaterini S. Genikomsou [3]

[1] Politécnico, Universidad San Francisco de Quito, Quito 170901, Ecuador
[2] Concrete Structures, Department of Engineering Structures, Civil Engineering and Geosciences, Delft University of Technology
[3] Queen's University, Kingston, ON, Canada
* Correspondence: danielvargas2901@gmail.com; Tel.: +593 999 757 470

Abstract: Eccentric punching shear can occur in concrete slab-column connections when the connection is subjected to shear and unbalanced moments. Typically, this situation results in edge and corner columns and is thus a common practical case. However, most punching experiments in the literature are concentric punching shear. This paper presents a developed database of eighty-eight experiments of flat slabs under eccentric punching shear, including a summary of the testing procedure of each reference and a description of the slab specimens. Additionally, a linear finite element analysis of all the specimens is included to determine the relevant sectional shear forces and moments. Finally, the ultimate shear stresses from the database experiments are compared to the shear capacities determined with ACI 318-19, Eurocode 2 NEN-EN 1992-1-1:2005, and the Model Code 2010. The comparison shows that the Model Code 2010 is the most precise in the predictions with an average tested over predicted ratio of 0.96 and a coefficient of variation of 27.96%. It can be concluded that this study represents the inconsistencies of the currently used design methods and the lack of experimental information.

Keywords: database; eccentric punching shear; experiments; flat slab; punching; reinforced concrete; shear

1. Introduction

Reinforced concrete flat slab floor systems are an interesting solution for building design due to the simplicity of the construction process and the associated economic advantages. Nevertheless, a difficulty lies in the uncertainty of predicting the slab-column connection behavior and capacity when lateral loads or unbalanced gravity loads cause the transfer of moments between the slab and the column [1]. Such moments can also be caused by asymmetrical spans, creep, and differential shrinkage between two continuous slabs [2], [3].

An important number of collapses caused by punching failure have been reported throughout the years, which gained the attention of researchers and practitioners [3]. One example is the collapse of the underground parking garage in Gretzenbach, Switzerland in November 2004 [4]. The collapsed structure had no shear reinforcement; only column capitals were provided for shear enhancement. This collapse caused the deaths of seven men.

Typically, the most critical slab-column connections are located on corners and edges as these connections are subjected to moment transfer and eccentric loading. However, these are less studied in comparison with internal slab-column connections under concentric loads.

The first comprehensive studies on punching shear were made in the 1960s by Kinnunen and Nylander [5], but their mechanical models resulted in complicated expressions, which the codes makers found unpractical to use [6]. Instead, empirical expressions

Preprints (www.preprints.org) | NOT PEER-REVIEWED | Posted: 21 June 2022 doi:10.20944/preprints202206.0289.v1

based on the available test results were developed for the development of the code provisions. Given that there is a lack of experimental information on eccentric punching shear on large-scale flat slabs, it becomes difficult to provide a satisfactory design expression [2]. To account for eccentric loading, the ACI 318-19 and the Eurocode 2 EN 1992-1-1:2005 models consider the shear stress on the critical perimeter [7], [8]. This perimeter is at a distance *d*/2 from the column in ACI 318-19, and at the same distance, but with rounded corners, in *fib* Model Code 2010. Eurocode 2 uses a perimeter at a distance 2*d* from the column and the perimeter has rounded corners as well. On the other hand, the *fib* Model Code 2019 [9] uses a reduction of the critical perimeter.

This work aims to present a wider view of the problem by compiling and analyzing experiments on eccentric punching shear from literature. The analysis of the compiled experiments can be used to examine the performance of the currently available building codes and identify which types of experiments would be a valuable contribution to the body of knowledge. Additional experiments could be used to refine and improve the existing models.

This article compiles 88 experiments on flat slabs in eccentric punching shear. Vertical, horizontal, and combined loading setups are reported in the literature. Both slabs with and without shear reinforcement are included in the developed database. Internal forces of the slabs for the maximum applied load, i.e., at the onset of punching shear failure, are typically not available in the references. To complete the missing information, a linear finite element model of each experiment is made. The experimental shear capacities from the database are then compared to the strengths predicted by the design expressions found in ACI 318-19 [7], Eurocode 2 NEN-EN 1992-1-1:2005 [8], and the *fib* Model Code 2010 [9].

2. Methods

2.1. Overview of code provisions

2.1.1. ACI-318-19

The punching shear provisions from ACI 318-19 are based on empirical equations derived from test results from the work of Moe [10] and ACI-ASCE Committee 426 [11]. The ACI 318-19 method is based on the maximum shear stress v_u on the critical perimeter b_o of the slab, which is located at 0.5 *d* from the face of the column, where *d* is the average slab effective depth. The maximum shear stress v_u should not exceed the nominal shear strength of the slab v_n. Figure 1 is a sketch of the shear stress produced by axial load and moment transfer on an internal slab column connection [1].

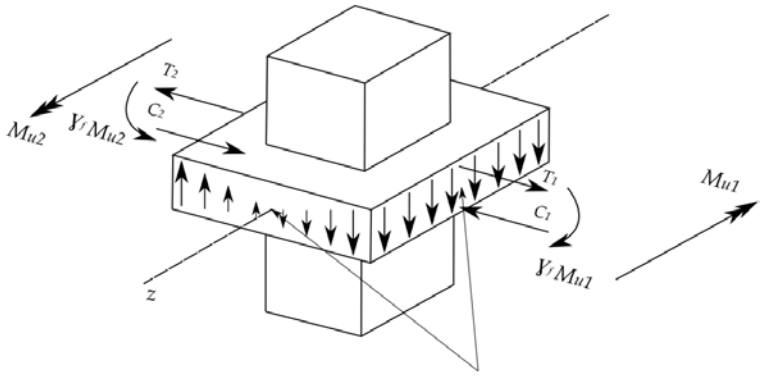

(**a**)

Preprints (www.preprints.org) | NOT PEER-REVIEWED | Posted: 21 June 2022 doi:10.20944/preprints202206.0289.v1

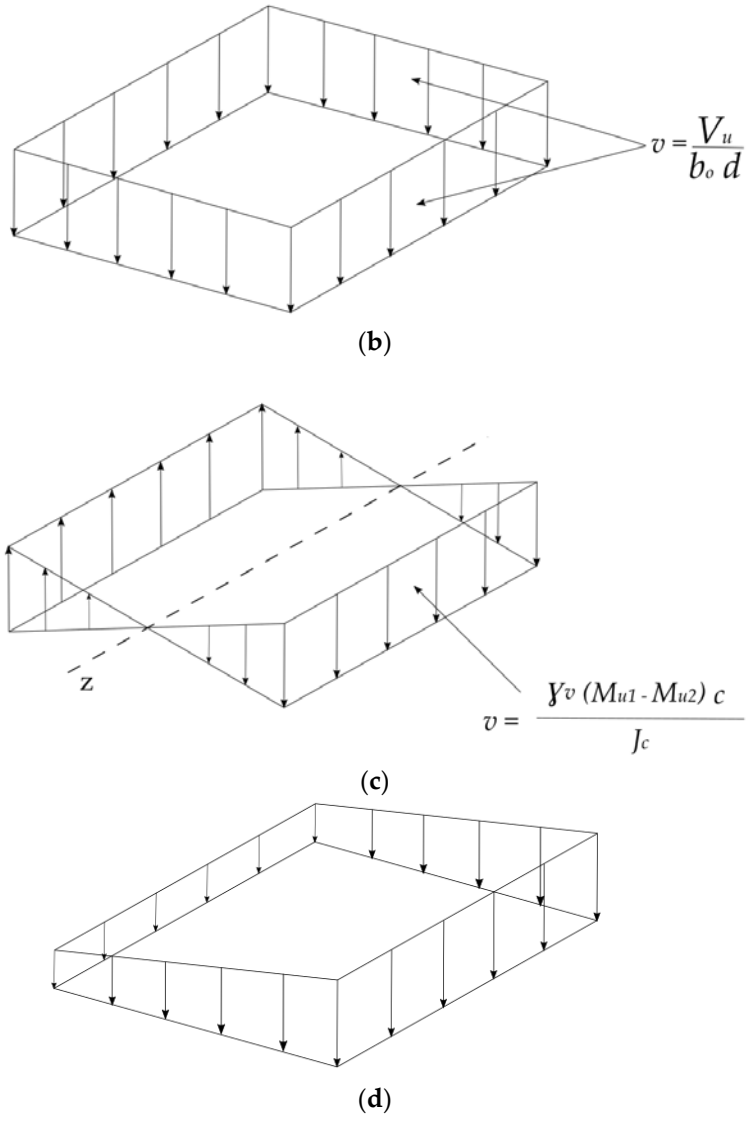

Figure 1. Shear stress produced by applied load and moment transfer, modified from [1]: (**a**) transfer of unbalanced moments to column; (**b**) shear stress caused by direct shear; (**c**) shear stress caused by unbalanced moments; (**d**) total shear stress: sum of (**b**) and (**c**).

MacGregor and Wight [1] define v_u using the following equation:

$$v_u = \frac{V_u}{b_o d} \pm \frac{\gamma_v M_u c}{J_c} \quad (1)$$

where V_u is the factored shear being transferred from the slab to the column acting on the centroid of the critical section; c is the distance from the centroid of the critical section to the point where the shear stress is calculated; J_c in the polar moment of inertia of the critical section and $\gamma_v M_u$ is the fraction of moment transferred by the eccentricity of shear, with γ_v as follows:

$$\gamma_v = 1 - \gamma_f \quad (2)$$

where γ_f is the fraction of moment transmitted by flexure:

$$\gamma_f = \frac{1}{1 + \left(\frac{2}{3}\right)\sqrt{\frac{b_1}{b_2}}} \quad (3)$$

Preprints (www.preprints.org) | NOT PEER-REVIEWED | Posted: 21 June 2022 doi:10.20944/preprints202206.0289.v1

where b_1 is the total width of the critical section measured perpendicular to the axis about which the moment acts, and b_2 is the total width parallel to the axis [1]. Figure 2 shows a sketch of the critical perimeter of an interior, edge, and corner slab-column connection.

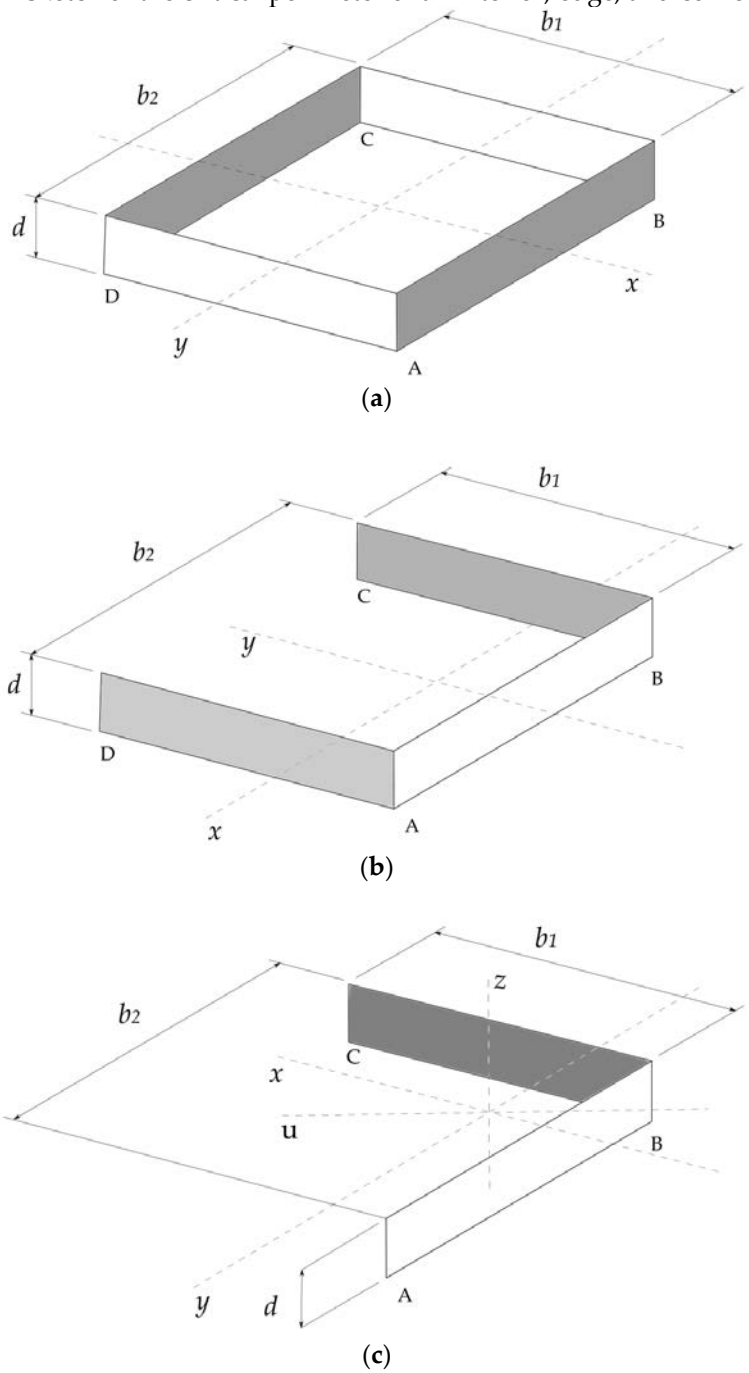

Figure 2. Critical perimeter of an interior, edge, and corner slab-column connections, modified from [1]: (**a**) interior slab-column connection; (**b**) edge slab-column connection; (**c**) corner slab-column connection.

The ultimate shear capacity v_n is calculated as follows, with v_u as determined by Eq. (1):

$$v_n = v_c + v_s \geq v_u \tag{4}$$

According to ACI 318-19 section 22.6.5.2 in slabs without reinforcement, the shear stress shall not exceed the least of the following three expressions, with f'_c in [MPa] [7]:

Preprints (www.preprints.org) | NOT PEER-REVIEWED | Posted: 21 June 2022 doi:10.20944/preprints202206.0289.v1

$$v_c = 0.33\lambda_s\lambda\sqrt{f_c'} \tag{5}$$

$$v_c = 0.17\left(1 + \frac{2}{\beta}\right)\lambda_s\lambda\sqrt{f_c'} \tag{6}$$

$$v_c = 0.083\left(2 + \frac{\alpha_s d}{b_o}\right)\lambda_s\lambda\sqrt{f_c'} \tag{7}$$

the value of α_s is 40 for interior columns, 30 for edge columns, and 20 for corner columns; λ_s is the size effect modification factor, λ is the lightweight factor; and β is the ratio of long to short column sizes [7].

The contribution of the shear reinforcement v_s is determined as:

$$v_s = \frac{A_v f_{yt}}{b_o s} \tag{8}$$

where A_v is the sum of the area of all legs of reinforcement on the peripheral line that is geometrically like the perimeter of the column section, f_{yt} is the yield strength of the transverse reinforcement and s is the spacing of transversal reinforcement [7].

Section 22.6.6.1 [7] indicates that the value of v_c for shear-reinforced slabs shall not exceed the following:

$$v_c = 0.17\lambda_s\lambda\sqrt{f_c'} \tag{9}$$

$$v_c = 0.25\lambda_s\lambda\sqrt{f_c'} \tag{10}$$

$$v_c = \left(0.17 + \frac{0.33}{\beta}\right)\lambda_s\lambda\sqrt{f_c'} \tag{11}$$

$$v_c = \left(0.17 + \frac{0.083\alpha_s d}{b_o}\right)\lambda_s\lambda\sqrt{f_c'} \tag{12}$$

Equation (9) is used for stirrup reinforcement and equations (10-12) are used for headed shear stud reinforcement, where the least of them shall be taken. When shear reinforcement is used, the critical perimeter b_o shall be taken outside the reinforced section as illustrated in Figure 3 [7].

Preprints (www.preprints.org) | NOT PEER-REVIEWED | Posted: 21 June 2022 doi:10.20944/preprints202206.0289.v1

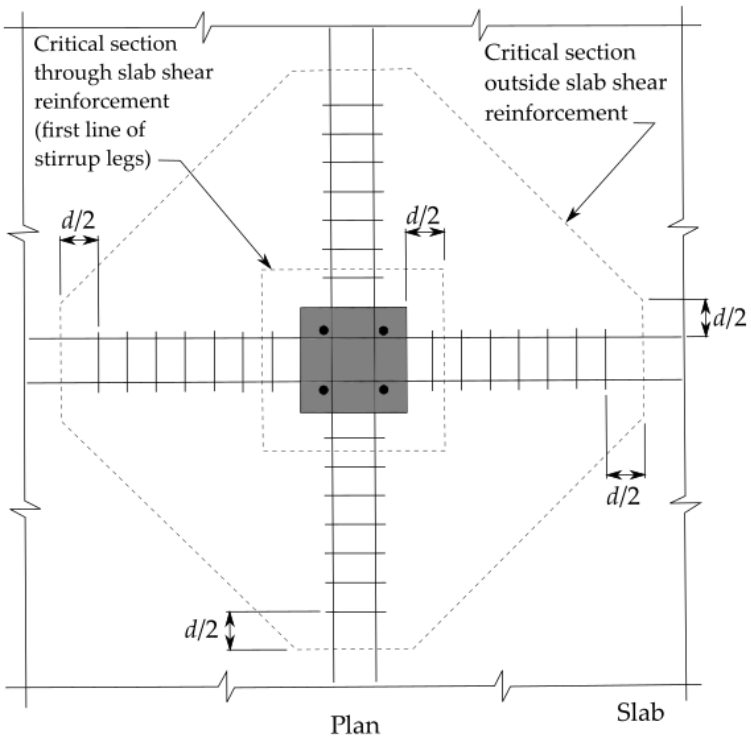

(**a**)

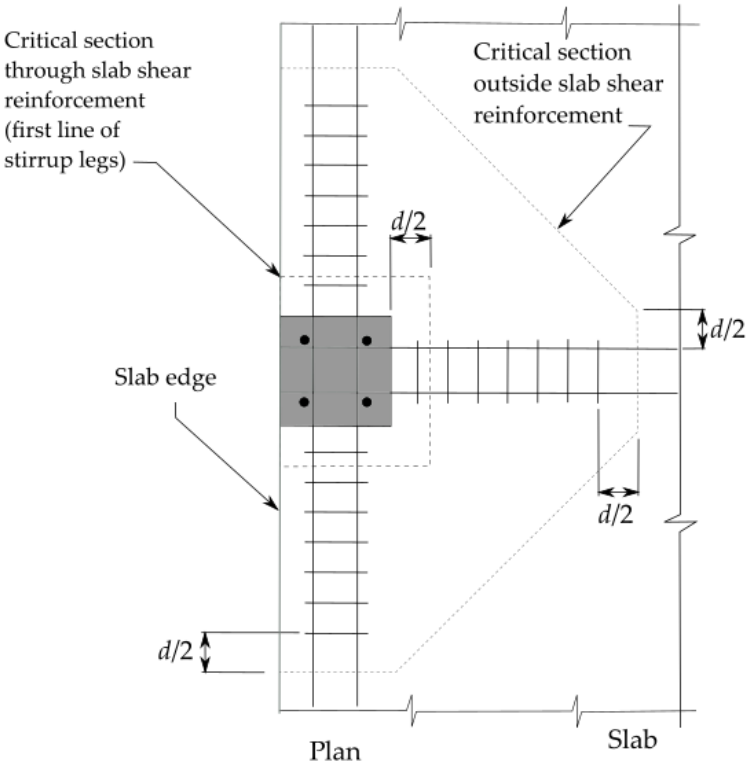

(**b**)

Preprints (www.preprints.org) | NOT PEER-REVIEWED | Posted: 21 June 2022 doi:10.20944/preprints202206.0289.v1

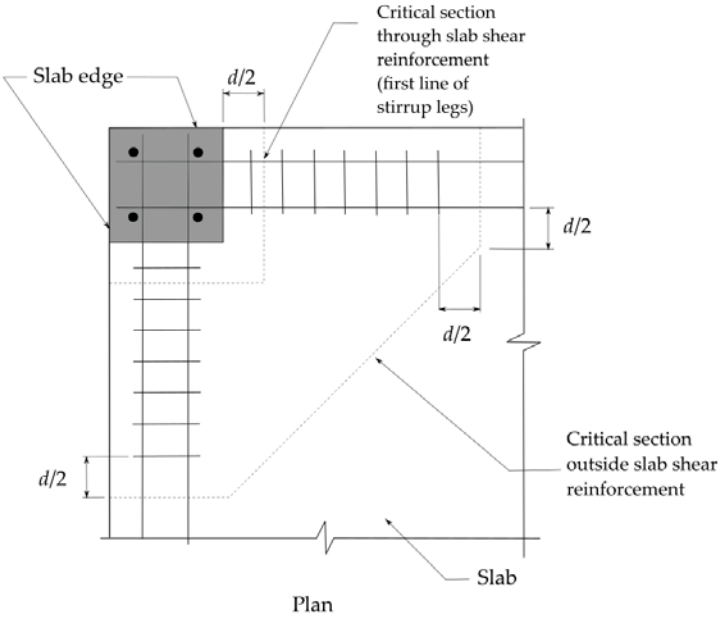

(**c**)

Figure 3. Critical perimeter for a shear reinforced interior, edge, and corner slab-column connection, modified from [7]: (a) interior slab-column connection; (b) edge slab-column connection; (c) corner slab-column connection.

2.1.2. NEN-EN 1992-1-1:2005

The punching shear provisions of NEN-EN 1992-1-1:2005 contain empirical equations for the concrete contribution to the two-way shear capacity. It is assumed that the concrete contribution to the shear capacity is equal for one-way shear (beam shear) and two-way shear (punching shear).

According to the provisions of NEN-EN 1992-1-1:2005 punching shear is checked at the basic control perimeter U_1 [8]. The basic control perimeter U_1 is located at $2d$ from the loaded area, with d the average effective depth of the slab. Figure 4 shows the basic control perimeter for an interior, edge, and corner slab-column connection [8]. Note that rounded corners are used for the perimeter.

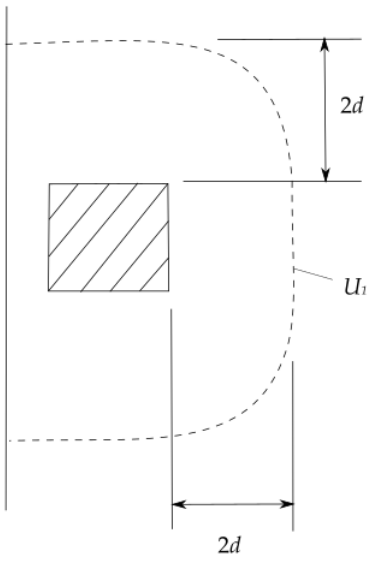

(**a**)

Preprints (www.preprints.org) | NOT PEER-REVIEWED | Posted: 21 June 2022 doi:10.20944/preprints202206.0289.v1

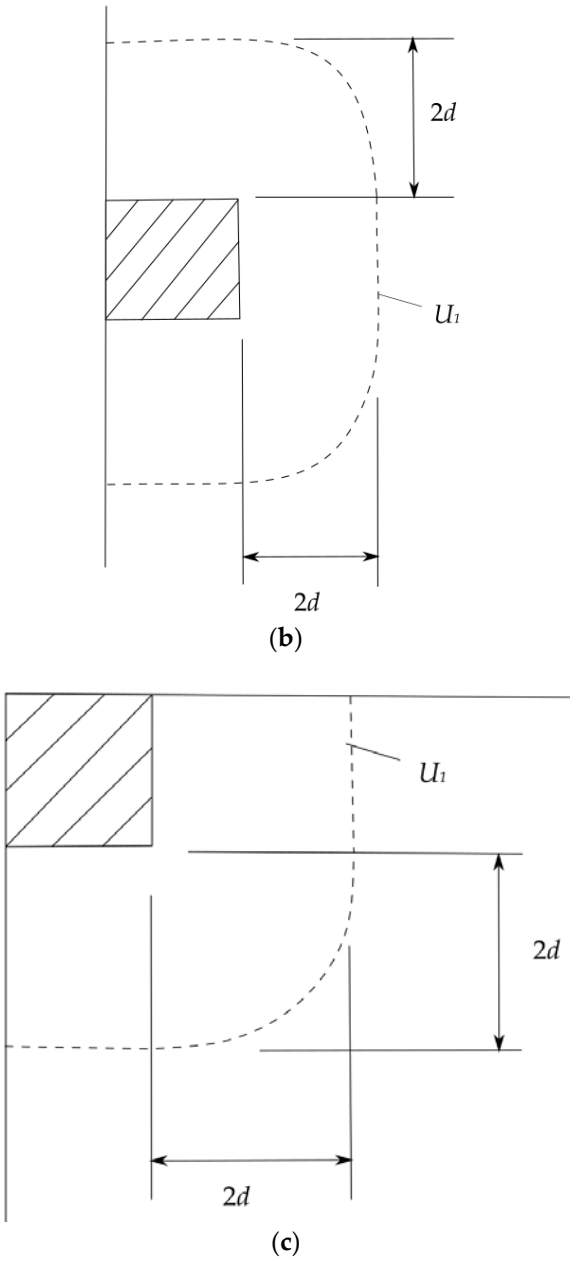

Figure 4. Basic control perimeter for an interior, edge, and corner slab-column connection, modified forms [8]: (a) interior slab-column connection; (b) edge slab-column connection; (c) corner slab-column connection.

Punching shear is evaluated based on the following stresses: $v_{Rd,c}$ the design value of the punching shear resistance of a slab without punching shear reinforcement, $v_{Rd,s}$ the value of the punching shear resistance of a slab with punching shear reinforcement, and v_{Ed} the maximum shear stress along the control section. If $v_{Ed} \leq v_{Rd,c}$ punching shear reinforcement is not necessary. If the support reaction is eccentric with respect to the control perimeter, the maximum shear stress is:

$$v_{Ed} = \beta_{EC} \frac{V_{Ed}}{U_1 d} \tag{13}$$

$$\beta_{EC} = 1 + k_c \frac{M_{Ed}}{V_{Ed}} \frac{U_1}{W_1} \tag{14}$$

 doi:10.20944/preprints202206.0289.v1

where W_1 represents the shear distribution on the control perimeter, V_{Ed} is the design value of the sectional shear force, M_{Ed} is the design value of the sectional bending moment, and k_c is a coefficient on the ratio between the column dimensions given by Table 6.1 of NEN-EN 1992-1-1:2005 [8]. A few values of k_c are 0.6 for a c_1/c_2 ratio of 1.0 and 0.70 for a c_1/c_2 ratio of 2.0, where c_1 and c_2 are the dimensions of the critical perimeter, see Figure 5. W_1 is calculated as:

$$W_1 = \int_0^{U_i} |e| dl \tag{15}$$

where U_i is the length of the control perimeter under consideration, dl is a length increment of the perimeter, and e is the distance of dl from the axis about which the moment M_{Ed} acts [8]. Figure 5 shows the shear distribution due to an unbalanced moment at a slab-column connection, indicating that the Eurocode approach assumes a fully plastic distribution of the shear stresses.

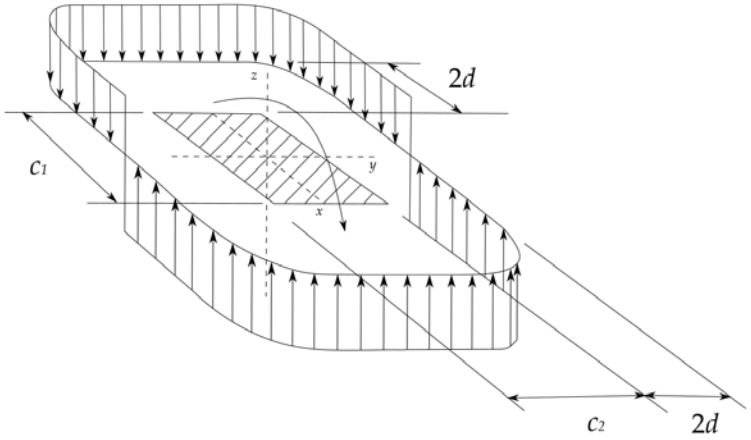

Figure 5. Shear distribution due to an unbalanced moment at a slab-column connection, modified from [8].

For an internal rectangular column where the loading is eccentric to both orthogonal axes, β_{EC} shall be calculated as follows:

$$\beta_{EC} = 1 + 1.8\sqrt{\left(\frac{e_y}{b_x}\right)^2 + \left(\frac{e_x}{b_y}\right)^2} \tag{16}$$

where e_y and e_x are the eccentricities M_{Ed}/V_{Ed} along the axes y and x respectively and b_x and b_y are the dimensions of the control perimeter. For edge slab-column connections, where the eccentricity is perpendicular to the slab edge is towards the interior and there is no eccentricity parallel to the edge, the control perimeter may be reduced to U_1^* as illustrated in Figure 6a. For corner slab-column connections, where the eccentricity is towards the interior of the slab, the control perimeter may be reduced to U_1^* as illustrated in Figure 6b [8].

Preprints (www.preprints.org) | NOT PEER-REVIEWED | Posted: 21 June 2022 doi:10.20944/preprints202206.0289.v1

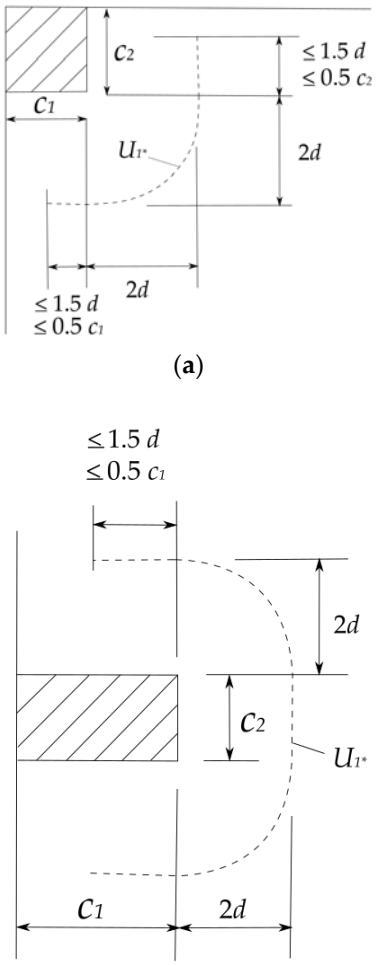

Figure 6. Reduced basic control perimeter, modified from [8]: (a) edge slab-column connection; (b) corner slab-column connection.

For edge slab-column connections, if there are eccentricities in both orthogonal directions, β_{EC} shall be calculated as:

$$\beta_{EC} = \frac{U_1}{U_1^*} + k_c \frac{U_1}{W_1} e_{par} \tag{17}$$

where e_{par} is the eccentricity parallel to the slab edge. For corner column connections, where the eccentricity is toward the interior of the slab, β_{EC} shall be calculated as:

$$\beta_{EC} = \frac{U_1}{U_1^*} \tag{18}$$

if the eccentricity is towards the exterior, β_{EC} shall be calculated using equation Eq. (16).

The punching shear resistance of slabs without shear reinforcement, $v_{Rd,c}$ is calculated as:

$$v_{Rd,c} = C_{Rd,c} k (100 \rho_l f_{ck})^{\frac{1}{3}} \geq v_{min} \tag{19}$$

with $v_{Rd,c}$ taken as $0.18/\gamma_c$, with γ_c the material factor for concrete ($\gamma_c = 1.5$), and k the size effect factor, calculated with the following expression, with d in [mm],

Preprints (www.preprints.org) | NOT PEER-REVIEWED | Posted: 21 June 2022 doi:10.20944/preprints202206.0289.v1

$$k = 1 + \sqrt{\frac{200}{d}} \leq 2 \tag{20}$$

the reinforcement ratio is the geometric average of the reinforcement ratio in the y (ρ_{ly}) and x (ρ_{lx}) direction:

$$\rho_l = \sqrt{\rho_{lx} \cdot \rho_{ly}} \tag{21}$$

the lower bound of the shear capacity is a nationally determined parameter, with a recommended expression for v_{min} as:

$$v_{min} = 0.035 k^{3/2} f_{ck}^{1/2} \tag{22}$$

The punching shear resistance of slabs with shear reinforcement is calculated as:

$$v_{Rd,cs} = 0.75 v_{Rd,c} + 1.5 \left(\frac{d}{s_r}\right) A_{sw} f_{ywd,ef} \left(\frac{1}{U_1 d}\right) \sin \alpha \tag{23}$$

where A_{sw} is the area of one perimeter of shear reinforcement around the column, s_r is the radial spacing of perimeters of shear reinforcement, $f_{ywd,ef}$ is the effective design strength of the punching shear reinforcement and α is the angle between shear reinforcement and the horizontal plane of the slab.

2.1.3. Model Code 2010

The *fib* Model Code 2010 punching shear provisions are based on the Critical Shear Crack Theory [10], [12], [13]. The design shear demand V_{Ed} acts on the basic control perimeter $b_{1,MC}$, at $0.5d_v$ from the supported area, where d_v is the effective depth of the slab. Figure 9 illustrates the basic control perimeter for different supported areas.

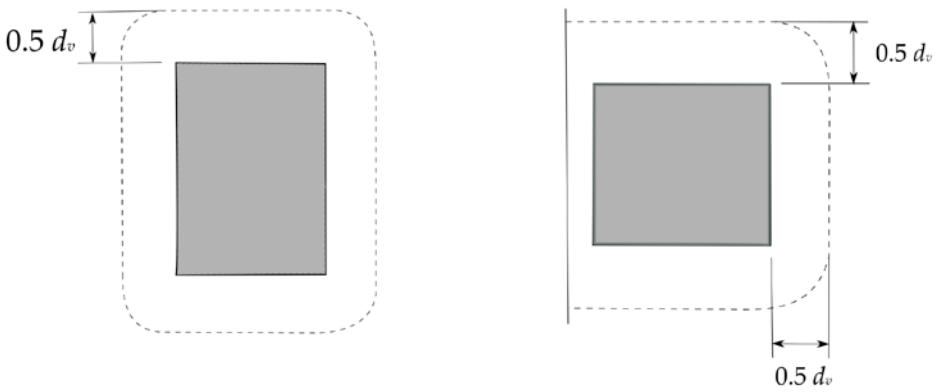

(**a**) (**b**)

Figure 9. Basic control perimeter, modified from [9]: (a) interior column; (b) edge slab-column connection.

Then, for calculating the punching shear resistance of the slab, a shear-resisting control perimeter b_0 is used. This perimeter accounts for the non-uniform distribution of shear forces along $b_{1,MC}$, which can be caused by concentrations of the shear forces due to moment transfer between the slab and the supported area because of eccentricities in the load application [9]. Figure 8 illustrates the eccentricity of the resultants [9].

Preprints (www.preprints.org) | NOT PEER-REVIEWED | Posted: 21 June 2022 doi:10.20944/preprints202206.0289.v1

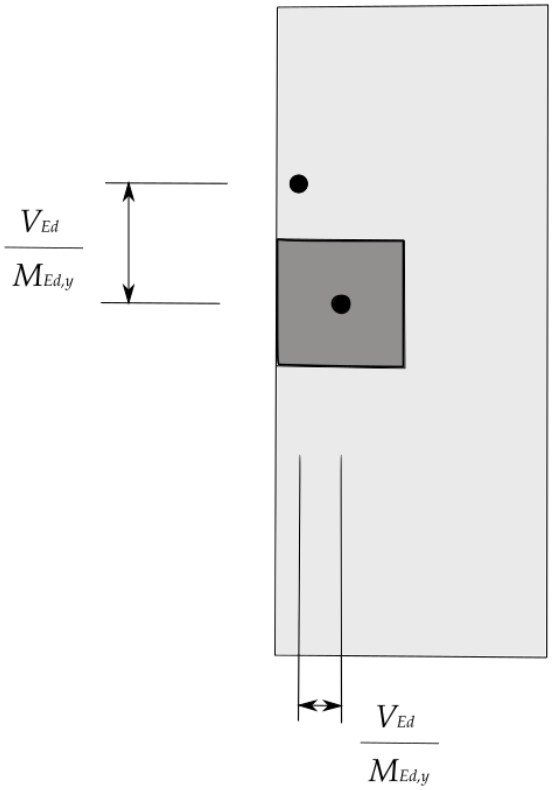

Figure 8. Resultant of shear forces, modified from [9].

The control perimeter b_0 is determined as:

$$b_0 = k_e b_{1,MC} \tag{24}$$

The factor k_e represents the coefficient of eccentricity:

$$k_e = \frac{1}{1 + \frac{e_u}{b_u}} \tag{25}$$

where e_u is the eccentricity of the resultant shear forces with respect to the centroid of $b_{1,MC}$, and b_u is the diameter of a circle with the same area as the region inside $b_{1,MC}$.

The punching shear resistance V_{Rd} is calculated as:

$$V_{Rd} = V_{Rd,c} + V_{Rd,s} \geq V_{Ed} \tag{26}$$

the design shear resistance attributed to the concrete is calculated using the following expression, with the compressive strength of the concrete, f_{ck}, in [MPa]:

$$V_{Rd,c} = k_\psi \frac{\sqrt{f_{ck}}}{\gamma_c} b_0 d_v \tag{27}$$

k_ψ is a parameter that depends on the rotations of the slab and shall be calculated as:

$$k_\psi = \frac{1}{1.5 + 0.9 k_{dg} \psi d} \leq 0.6 \tag{28}$$

where d is the mean value of the effective depth of the slab for x and y directions, and k_{dg} shall be calculated as follows, with d_g in [mm]:

$$k_{dg} = \frac{32}{16 + d_g} \geq 1.15 \tag{29}$$

where d_g is the maximum aggregate size.

Preprints (www.preprints.org) | NOT PEER-REVIEWED | Posted: 21 June 2022 doi:10.20944/preprints202206.0289.v1

The design shear resistance attributed to the shear reinforcement is calculated as:

$$V_{Rd,s} = \sum A_{sw} k_e \sigma_{swd} \sin \alpha \quad (30)$$

where $\sum A_{sw}$ is the sum of the area of all the shear reinforcement acting on the zone between $0.35d_v$ and d_v, which has a length of $0.65d_v$, see Figure 9 [9].

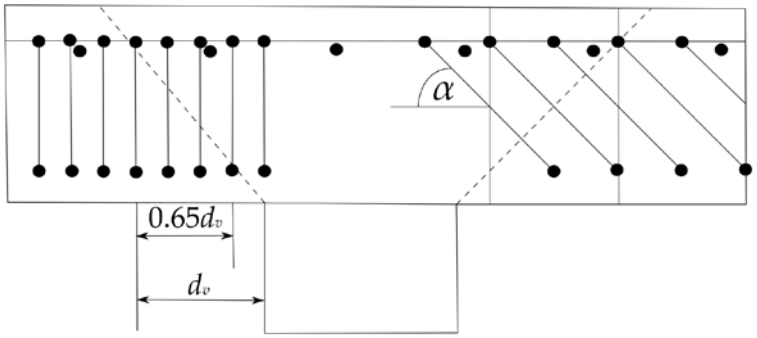

Figure 9. Shear reinforcement acting at failure, based on [9].

The stress σ_{swd} is calculated as:

$$\sigma_{swd} = \frac{E_s \psi}{6} \leq f_{ywd} \quad (31)$$

where f_{ywd} is the yield strength.

The load-rotation behavior of the slab is calculated as follows:

$$\psi = 1.5 \frac{r_s}{d} \frac{f_{yd}}{E_s} \left(\frac{m_{sd}}{m_{rd}}\right)^{1.5} \quad (32)$$

where r_s is the distance from the column axis to the line of contra-flexure of the radial bending moments; f_{yd} is the yield strength of the flexural reinforcement, E_s the modulus of elasticity of the flexural steel, m_{sd} the average moment per unit length for calculating flexural reinforcement in the support strip, and m_{Rd} is the average flexural strength per unit length in the support strip [9]. The values of the mechanical parameters in the formula can be calculated with different levels of approximation (LoA), where increasing levels of approximation indicate increasing precision but also increasing computational time and effort [6].

LoA I assumes that $m_{sd} = m_{Rd}$, which implies that the strength of the slab will be governed by its bending moment capacity. For regular slabs with a long over short side ratio $0.5 \leq L_x/L_y \leq 2.0$, r_s can be estimated as follows:

$$r_{sx} = 0.22L_x \; ; r_{sy} = 0.22L_y \quad (33)$$

Figure 10 illustrates L_x and L_y [9].

Preprints (www.preprints.org) | NOT PEER-REVIEWED | Posted: 21 June 2022 doi:10.20944/preprints202206.0289.v1

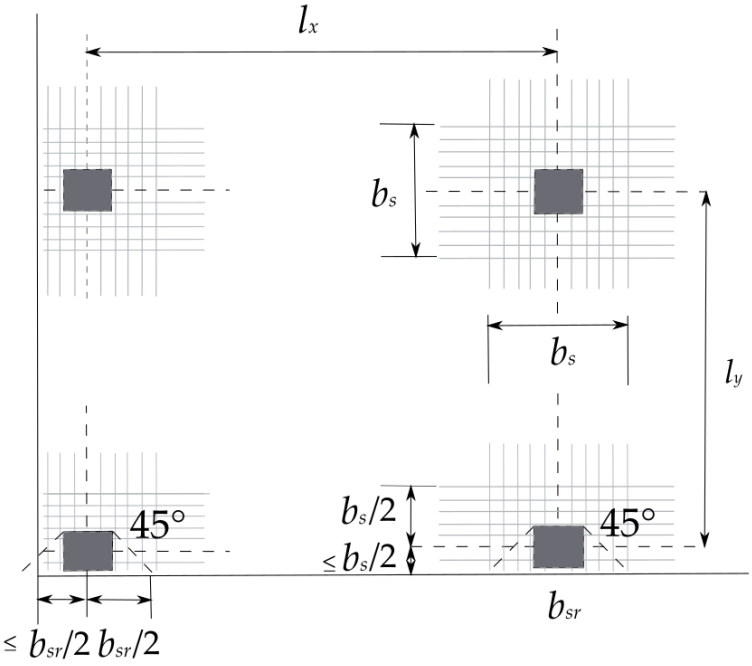

Figure 10. Slab dimensions and support strip dimensions, modified from [12].

LoA II includes a simplified estimation of m_{sd}. LoA III replaces the coefficient 1.5 in Eq. (32) by 1.2 if r_s and m_{sd} are calculated using a linear elastic model. LoA IV is based on a nonlinear analysis of the structure and it considers cracking, tension-stiffening effects, yielding of the reinforcement, and any other relevant nonlinear effects [9].

2.2 Database of eccentric punching shear experiments

2.2.1 Development of the database

The database developed for this study contains 88 experiments of eccentric punching shear on flat slabs with longitudinal reinforcement and with or without transverse shear reinforcement reported in the literature. The consulted references are by Albuquerque et al. [14], Hammill and Ghali [15], Narayani [16], Zaghlool [17], Anis [18], Hanson and Hanson [19], Moe [10], and Stamenkovic [20]. Tables A1-A7 present the database developed for this study. The full spreadsheet is available in the public domain in .xlsx format [21]. The notations used in this database are given in the "List of notations". Figure 11 illustrates the different slab geometries and slab-column connections found in the literature [14]–[16].

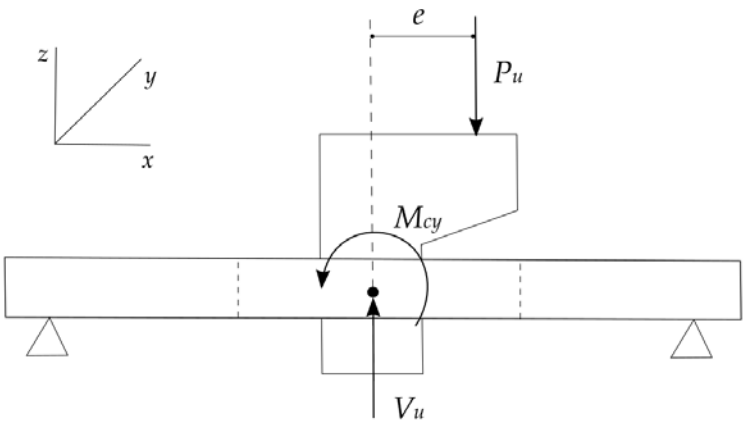

(**a**)

Preprints (www.preprints.org) | NOT PEER-REVIEWED | Posted: 21 June 2022 doi:10.20944/preprints202206.0289.v1

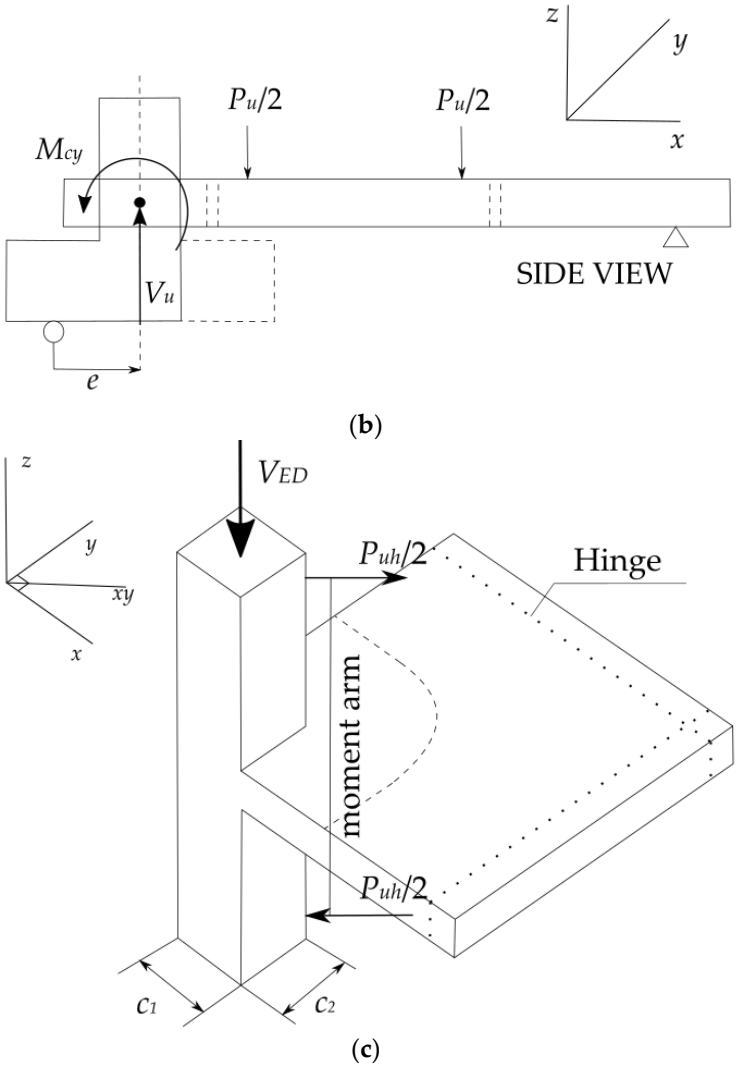

Figure 11. Slab geometries and test slab-column connection: (a) square interior slab-column connection [16]; (b) rectangular edge slab-column connection [14]; (c) square corner slab-column connection [15].

For references [2], [14], [15], [19], the age of the specimens at the time of testing was not provided, and thus it is assumed to be 28 days. For references [2], [10], [15], [18]–[20] the tensile strength of the concrete f_{ct} was not reported by the authors. To complete this information, the expression developed from Sarveghadi [22] was used:

$$f_{ct} = 0.76\sqrt{f_c} \tag{34}$$

with f_c the cylinder concrete compressive strength in [MPa].

For references [15], [16], [20]the modulus of elasticity of the flexural reinforcement was not provided; for [15], [20] it was assumed 200 GPa, and for [16] it was estimated from the stress-strain graph reported by the author.

References [14]–[16] present slabs with transverse shear reinforcement: stirrups, shear hats (see Figure 12), and studs were the shear reinforcement types found in these references.

Preprints (www.preprints.org) | NOT PEER-REVIEWED | Posted: 21 June 2022 doi:10.20944/preprints202206.0289.v1

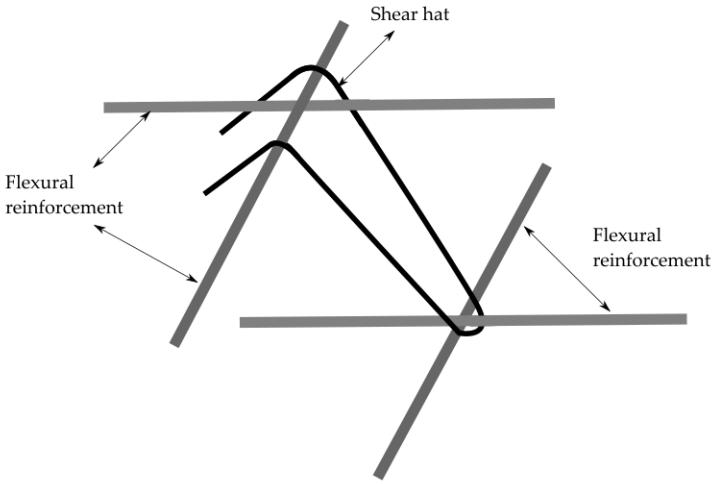

Figure 12. Shear hat setup, as used in [16].

For internal slab-column connections, references [2], [10], [16], [19] presented the ultimate load applied to the slab-column connection and its eccentricity; on the other hand, references [18], [20] reported the ultimate moment applied to the slab-column connection. Edge slab-column connections, references [14], [16], [19] presented the ultimate load applied to the slab-column connections and its eccentricity, and references [17], [20] reported the ultimate moment applied to the slab-column connection. Finally, for corner slab-column connections, [15], [17] reported the ultimate moment applied to the slab-column connection; in both references the test setup caused this moment to act diagonally on the slab. Figure 11c illustrates this type of loading. For the database, the diagonally applied moment was divided into its components in the x and y directions. All values in the database are presented in SI units. The information from [10], [17]–[20] was converted from U.S customary to SI units.

The FEM models were developed in Scia Engineer [23] as similar to the reported experiments as possible, including the contribution of the self-weight when testing occurred in the gravity direction (i.e., self-weight increases sectional shear). The results presented in Tables B1-B3 are the maximum internal forces of the slab at failure, measured on the punching perimeter described in the ACI 318-19 code [7]

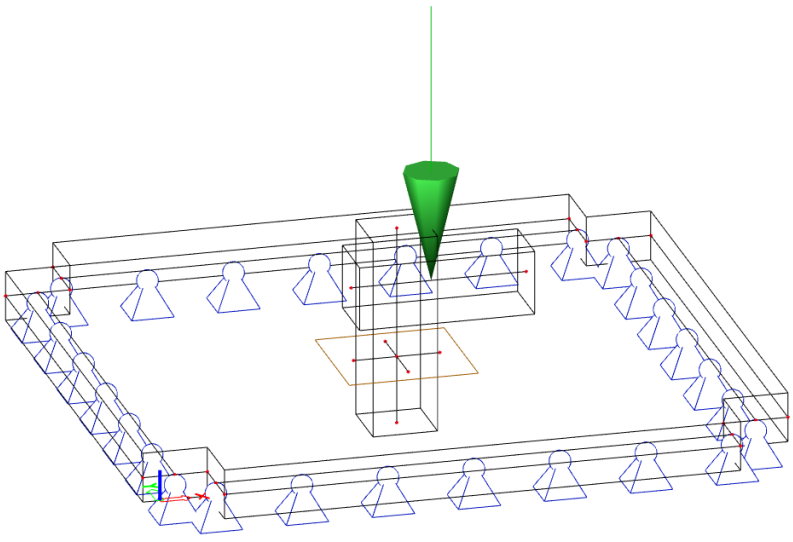

(**a**)

Preprints (www.preprints.org) | NOT PEER-REVIEWED | Posted: 21 June 2022 doi:10.20944/preprints202206.0289.v1

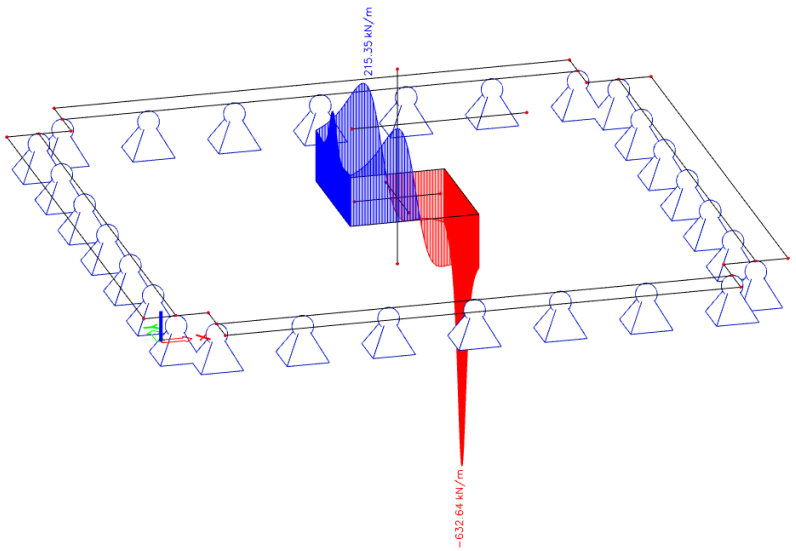

(**b**)

Figure 13. Example of Finite Element Analysis on a Narayani [16]specimen: (a) Applied loads in the model; (b) Internal shear stress acting on the critical perimeter, calculated from the applied load and the self-weight of the specimen.

2.2.2 Parameter ranges in the database

In this section, an evaluation of the distribution of the values of the parameters in the database is made. Table 1 gives the ranges of the most important parameters in the database. The value of ρ is either taken directly from the reference, where available, or calculated as the geometric average of the longitudinal and transverse reinforcement ratios.

Table 1. Ranges of parameters in the database

Parameter	Min	Max
L_x (mm)	914	3000
L_y (mm)	914	3000
h (mm)	76	180
d (mm)	56	151
ρ (%)	0.88%	2.23%
f_c (MPa)	16	59
d_g (mm)	10	38
a (mm)	416	2000
a_v (mm)	298	1850

Figure 14 shows the distribution of the most important parameters in the database. Figure 14a shows that the majority of the slabs are made of normal strength concrete. The developed database cannot be used to gain insight into the eccentric punching shear capacity of high-strength concrete slab-column connections. Figure 14b shows that a tensile reinforcement ratio in the range of 1.25%-1.50% was commonly used in the tested slabs. Typical slab designs use reinforcement ratios of 0.6% - 0.8%. None of the experiments in the database use these practical values, with most slabs to be over-reinforced in flexure to achieve a punching shear failure. The distribution of the average effective depth of the slab is presented in Figure 14c. This plot shows that at least half of the specimens had an effective depth d in the range 100 mm - 125 mm and another large portion of the specimens

Preprints (www.preprints.org) | NOT PEER-REVIEWED | Posted: 21 June 2022 doi:10.20944/preprints202206.0289.v1

had an effective depth close to 75 mm. The reported specimens are small-scale specimens that do not give us insights regarding the size effect for eccentric punching shear. Figure 14d shows the ratio between the shear span and the average effective depth a/d. The range of a/d in the experiments covers only situations in which no direct load transfer can occur, as such, for this database there is a consistency in the range of a/d. Figure 14e shows the maximum aggregate size values reported in the literature. The values reported are consistent with values shown in Figure 14c: relatively small maximum aggregate sizes are used for the fabrication of specimens with small depths.

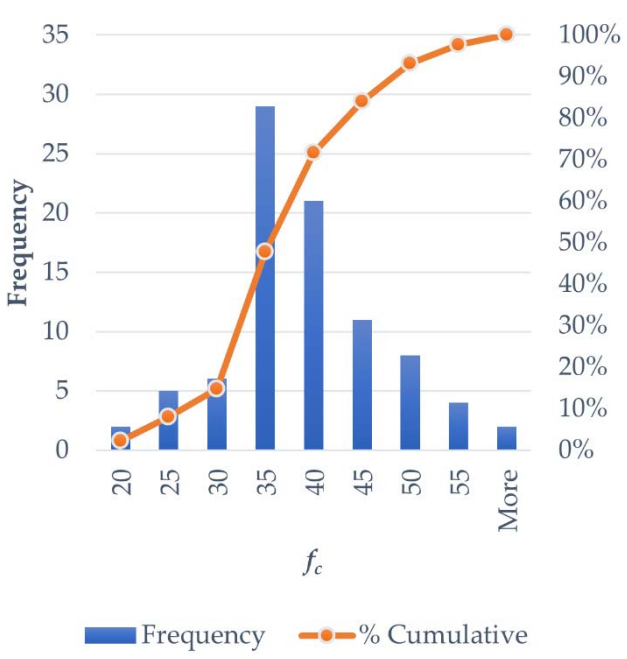

(a)

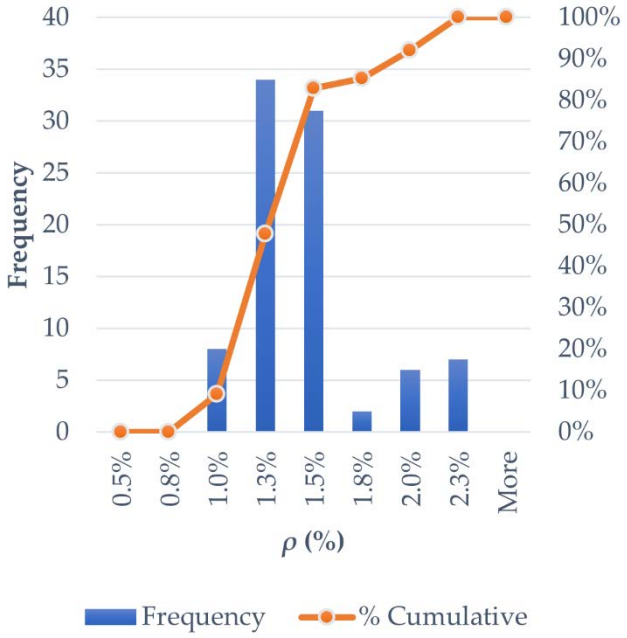

(b)

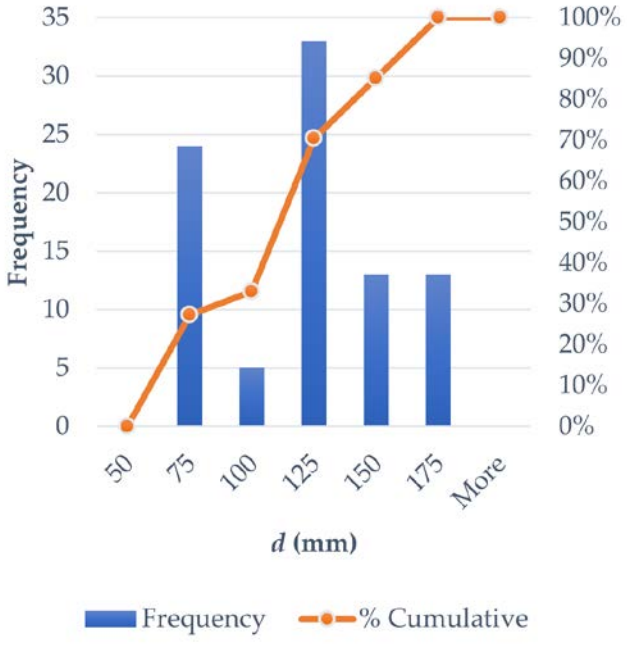

(c)

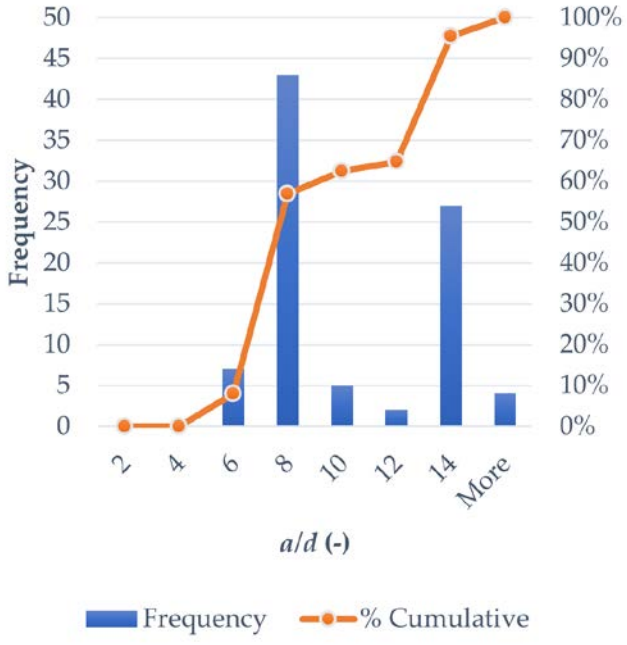

(d)

Preprints (www.preprints.org) | NOT PEER-REVIEWED | Posted: 21 June 2022 doi:10.20944/preprints202206.0289.v1

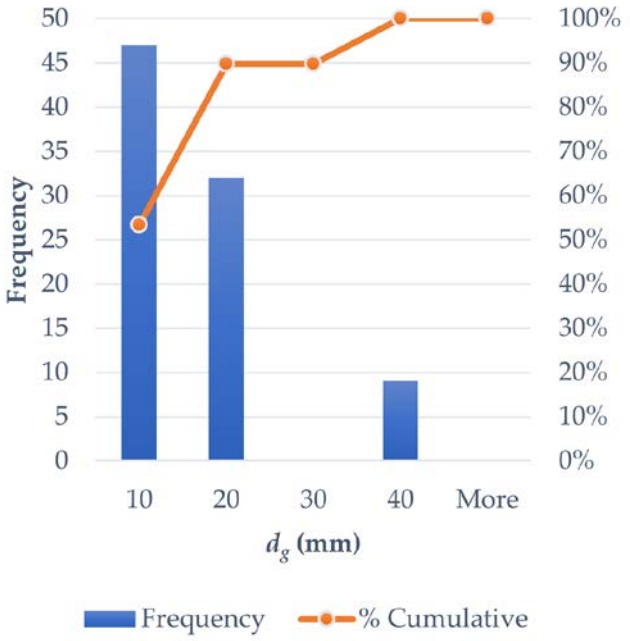

(e)

Figure 14. Distribution of the most important parameters in the database: (a) concrete compressive strength f_c; (b) tensile reinforcement ratio ρ; (c) effective depth d; (d) shear span to average effective depth ratio a/d; (e) maximum aggregate size d_g.

3. Results

3.1. Parameters studied

The raw data from the database are used to analyze the effect of different experimental parameters on the sectional shear stress at failure. The ACI 318-19 [7] expression (Eq. 1) is used for determining the shear stress on the perimeter v_u. Normalized shear stresses are used to discard the influence of the concrete compressive strength f_c. An analysis of the normalized shear stress to the square root and to the cubic root is made first. Figures 15a and 15b show the relation between the normalized shear strength and f_c and, as it can be seen, for the studied experimental results, normalizing the shear strength to the square root is to be preferred. A similar observation was made for the shear capacity of steel fiber reinforced concrete beams [24].

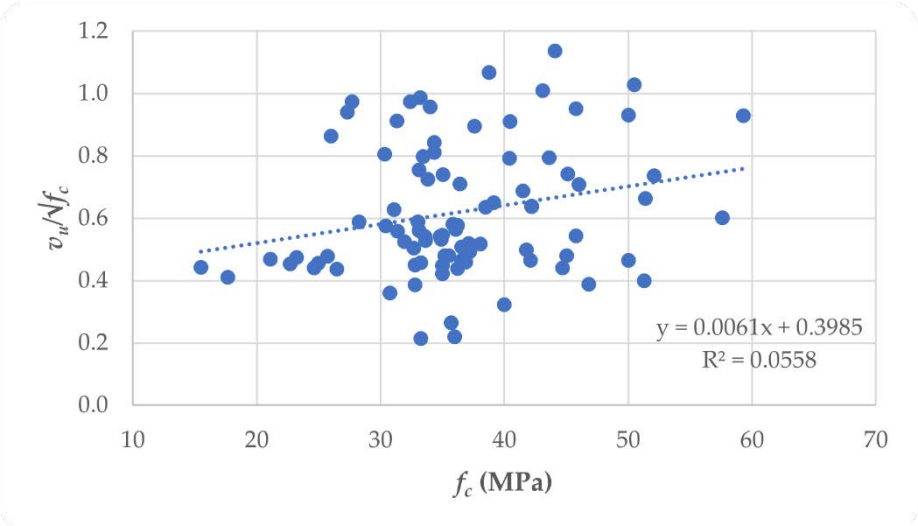

(a)

Preprints (www.preprints.org) | NOT PEER-REVIEWED | Posted: 21 June 2022 doi:10.20944/preprints202206.0289.v1

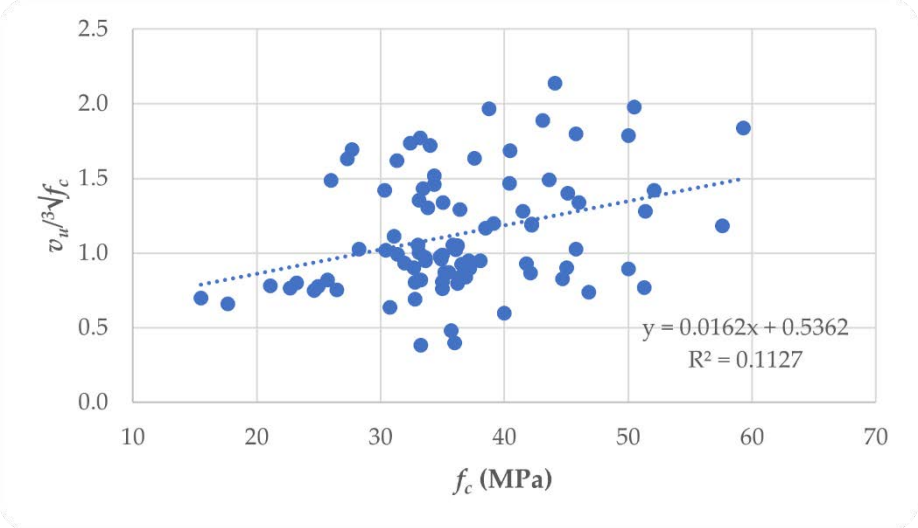

(b)

Figure 15. Normalized shear stresses to the concrete compressive strength: (a) normalized to the square root; (b) normalized to the cubic root.

Thus, the influence of different important parameters will be studied as a function of the shear stress normalized to the square root of f_c. Figure 16 shows the influence of the most important parameters on the shear stress normalized to the square root of f_c. Figure 16a shows the influence of the effective depth d on the normalized shear stress. For the specimens in the compiled database, the effective depth has some influence on the normalized shear stress as it increases with the normalized shear stress. However, experiments on slabs with a larger effective depth are not available, so this database cannot give insights regarding the size effect in eccentric punching shear. Figure 16b shows the influence of the reinforcement ratio ρ. Larger reinforcement ratios result in larger shear capacities, as expected. As more tension reinforcement is provided, the contribution of dowel action to the shear capacity increases, as reflected by the results from the database. Figure 16c shows the influence of the shear span to the effective depth a/d. For the experiments in the compiled database, this parameter had negligible influence on the normalized shear stress.

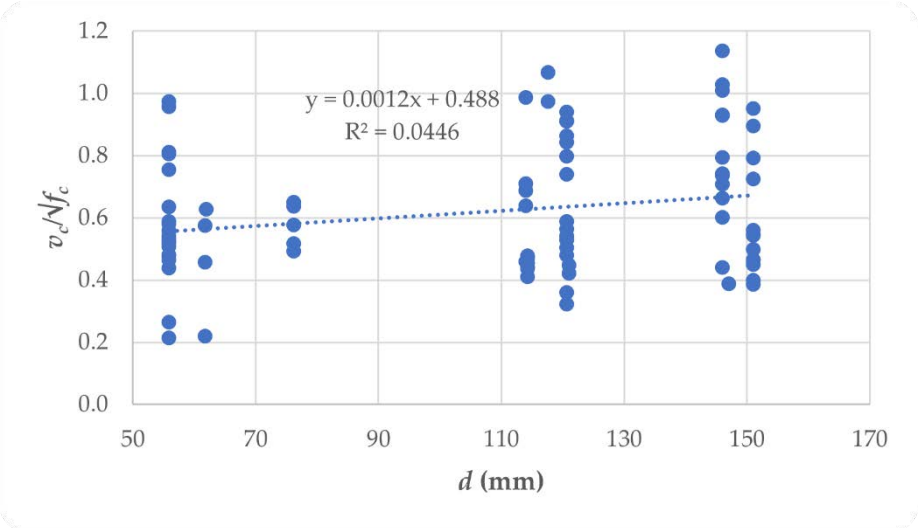

(a)

Preprints (www.preprints.org) | NOT PEER-REVIEWED | Posted: 21 June 2022 doi:10.20944/preprints202206.0289.v1

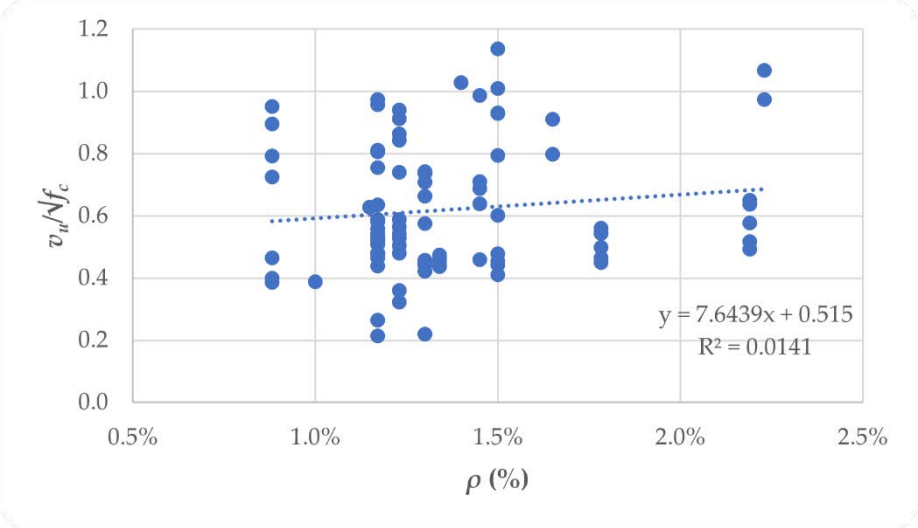

(b)

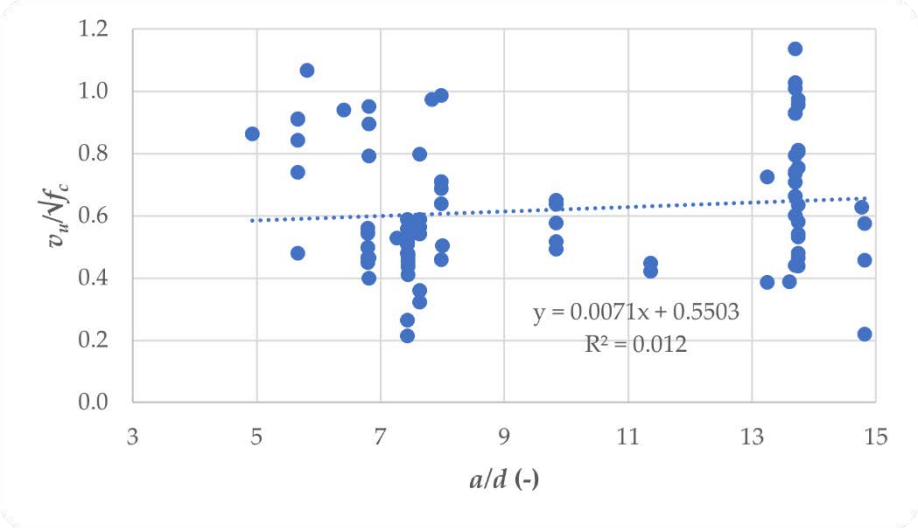

(c)

Figure 16. Parameter studies based on the normalized shear stress at failure of all entries in the database: (a) effective depth d; (b) longitudinal reinforcement ratio ρ; (c) shear span to depth ratio a/d.

3.2. Comparison to code predictions

The measured shear capacities from the database are then compared to the shear capacities predicted by three different codes: ACI 318-19 [7], NEN-EN 1992-1-1:2005 [8], and the *fib* Model Code 2010 [9]. Figure 17 shows the comparison between tested and predicted results, with the statistical properties of tested to predicted shear stresses in Tables 2-4. Figure 18 shows the comparison between the SCIA Engineer [23] FEM results, v_{FEM}, and predicted shear capacities v_{pred} for the ACI 318-19 [7], with the statistical properties of this comparison in Table 5. We compared the FEM results of the shear stress only to ACI 318-19 [7], as NEN-EN 1992-1-1:2005 and *fib* Model Code 2010 assume a plastic stress distribution on the punching perimeter. The ACI 318-19 [7], on the other hand, assumes a linear stress distribution. We compared to the results of the linear finite element analysis to check the alignment of the assumptions of linear behavior. The results for all the entries of the database are presented in Tables B1-B3. Some experiments use only moment transferred from the column and do not use a load on the slab. In these references, the NEN-EN 1992-1-1:2005 [8], and fib Model Code 2010 [9] models were not evaluated. Eq. (14) from NEN-EN 1992-1-1:2005 [8] uses the value of shear force applied to the slab column

Preprints (www.preprints.org) | NOT PEER-REVIEWED | Posted: 21 June 2022 doi:10.20944/preprints202206.0289.v1

connection for calculating the enhancement factor for eccentric shear, β_{EC}, so that the shear stress caused by unbalanced moment only cannot be determined. The same problem arises when applying Equations (24-25) from the *fib* Model Code 2010 [9]: the eccentricity e_u is calculated from the resultant shear forces applied to the slab-column connection.

When analyzing the specimens for references [18]–[20], the *fib* Model Code 2010 [9] model gave low tested to predicted values as a consequence of the maximum aggregate size and the effective depth in the expressions. Thus, the specimens of these references were not evaluated, as these specimens were outside of the scope of application of this code. The validation of the spreadsheet used for calculating the code predictions is available in the public domain [25].

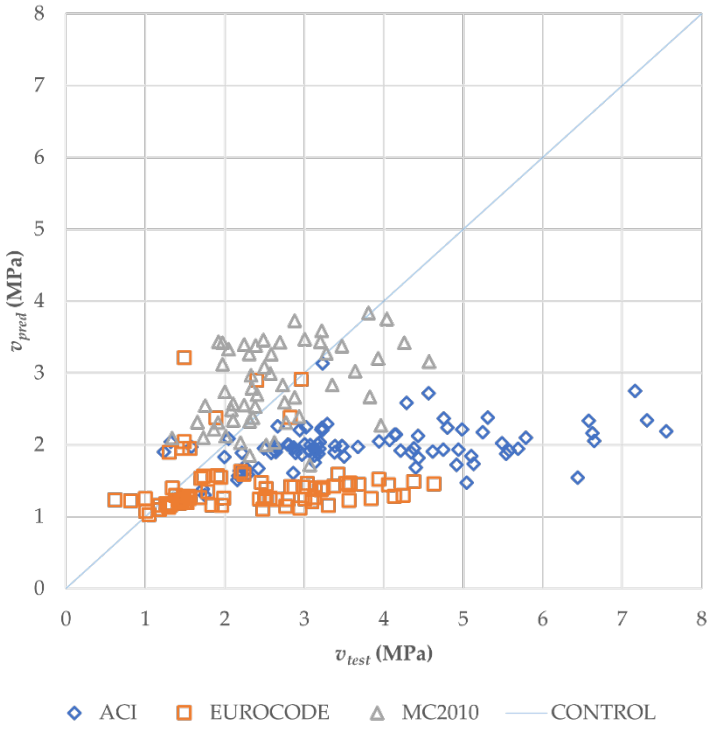

Figure 17. Comparison between experimental v_{test} and predicted shear capacities v_{pred} for 3 design methods from existing codes

Preprints (www.preprints.org) | NOT PEER-REVIEWED | Posted: 21 June 2022 doi:10.20944/preprints202206.0289.v1

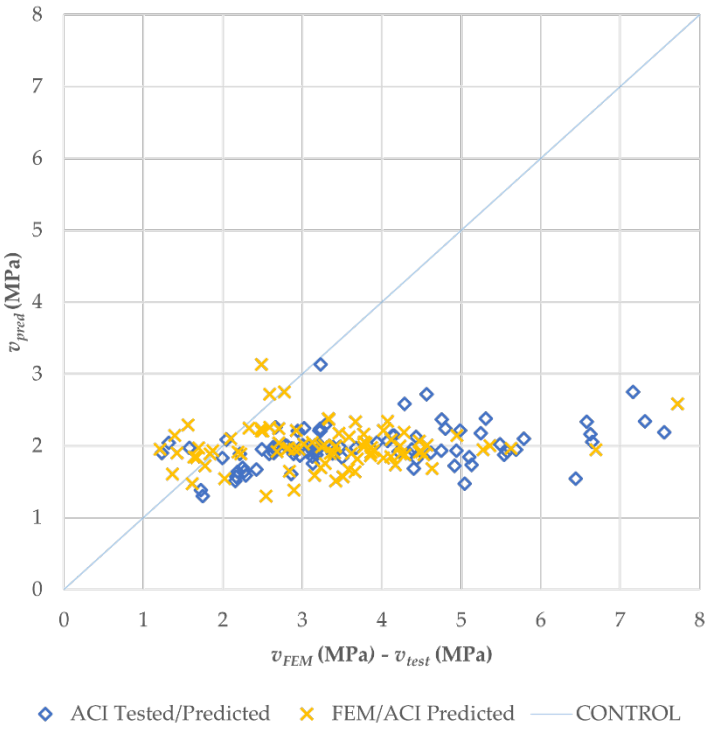

Figure 18. Comparison between the SCIA Engineer [23] FEM results to the predicted shear capacities for ACI 318-19 [7]

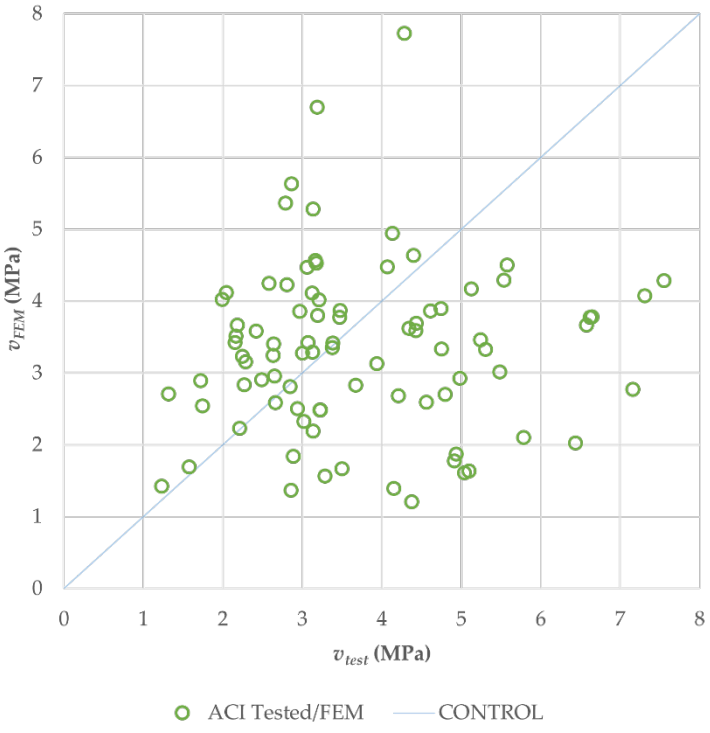

Figure 19. Comparison between the SCIA Engineer [23] FEM results and the shear stress for ACI 318-19 [7] calculated using Eq. (1)

Table 2. Statistic results from the comparison between the tested and predicted capacities, Part I. The number of specimens used for the evaluation is shown between brackets.

 doi:10.20944/preprints202206.0289.v1

All results			
	AVG	STD	COV (%)
ACI (88)	1.92	0.66	34.52
EC2 (68)	1.68	0.74	44.09
MC2010 (55)	0.96	0.27	27.96
Internal slab-column connections			
	AVG	STD	COV (%)
ACI (33)	1.42	0.31	21.79
EC2 (33)	1.23	0.55	44.43
MC2010 (17)	0.84	0.21	25.47
Edge slab-column connections			
	AVG	STD	COV (%)
ACI (41)	2.29	0.71	31.05
EC2 (37)	2.07	0.70	34.07
MC2010 (27)	1.03	0.29	28.50
Corner slab-column connections			
	AVG	STD	COV (%)
ACI (14)	2.00	0.30	14.95
EC2 (11)	1.74	0.65	37.18
MC2010 (11)	0.96	0.22	38.41

Table 3. Statistic results from the comparison between the tested and predicted capacities, Part II. The number of specimens used for the evaluation is shown between brackets.

Slabs without shear reinforcement			
	AVG	STD	COV (%)
ACI (75)	1.89	0.61	32.08
EC2 (55)	1.78	0.72	40.31
MC2010 (42)	1.02	0.26	24.98
Internal slab-column connections			
	AVG	STD	COV (%)
ACI (28)	1.42	0.28	19.95
EC2 (28)	1.31	0.40	30.26
MC2010 (12)	0.94	0.18	18.84
Edge slab-column connections			
	AVG	STD	COV (%)
ACI (35)	2.25	0.64	28.33
EC2 (31)	2.16	0.68	31.36
MC2010 (21)	1.09	0.29	27.13
Corner slab-column connections			
	AVG	STD	COV (%)
ACI (12)	1.76	0.55	31.04
EC2 (9)	1.96	0.47	23.80
MC2010 (9)	1.00	0.38	38.41

Preprints (www.preprints.org) | NOT PEER-REVIEWED | Posted: 21 June 2022 doi:10.20944/preprints202206.0289.v1

Table 4. Statistic results from the comparison between the tested and predicted capacities, Part III. The number of specimens used for the evaluation is shown between brackets.

Shear-reinforced slabs			
	AVG	STD	COV (%)
ACI (13)	2.06	0.94	45.39
EC2 (13)	1.14	0.63	55.19
MC2010 (13)	0.75	0.19	25.09
Internal slab-column connections			
	AVG	STD	COV (%)
ACI (5)	1.43	0.30	20.98
EC2 (5)	0.77	0.23	29.85
MC2010 (5)	0.61	0.04	6.76
Edge slab-column connections			
	AVG	STD	COV (%)
ACI (6)	2.52	1.10	43.54
EC2 (6)	1.58	0.69	43.55
MC2010 (6)	0.85	0.22	26.49
Corner slab-column connections			
	AVG	STD	COV (%)
ACI (4)	2.29	0.90	39.09
EC2 (2)	0.74	0.08	10.48
MC2010 (2)	0.78	0.01	1.74

Table 5. Statistic results from the comparison between SCIA Engineer [23] FEM results for the acting shear stress and the predicted shear capacities for ACI 318-19 [7]

	AVG	**STD**	**COV (%)**
All specimens	1.72	0.66	38.56
Internal slab-column connections	1.76	0.48	27.30
Edge slab-column connections	1.57	0.64	40.44
Corner slab-column connections	2.08	0.97	46.46

As can be observed in Table 2, ACI 318-19 [7] and NEN-EN 1992-1-1:2005 [8] tend to be on the conservative side in terms of the average tested to predicted shear stresses. The Model Code 2010 [9] has predicted shear capacities that are on average similar to the tested shear stress at failure (average = 0.96). Considering the overall results, the Model Code 2010 [9] also has the smallest coefficient of variation (COV = 27.96%) on the tested to predicted shear stresses. The tested to predicted values using NEN-EN 1992-1-1:2005 [8] show the lowest maximum value for one entry (0.47); however, the tested to predicted value using the Model Code 2010 [9] for this entry is small as well (0.58). The entry analyzed is named L5, from [16], is an internal slab column connection, reinforced in shear. See Table B1.

Whereas the other models consider only a part of the shear reinforcement, ACI 318-19 [7] considers all the shear reinforcement on the peripheral line that is geometrically like the perimeter of the column section. As a result, the predicted shear resistance according to ACI 318-19 [7] for shear-reinforced slab-column connections is significantly larger than the capacity predicted with the other methods, see Tables B1-B3. Comparing Tables 3 and 4, we can also observe a large increase in the COV for the ACI 318-19 [7] results from 32.08% for the case of slabs without shear reinforcement to 45.39% for those with shear reinforcement.

An increase in COV between slabs without and with shear reinforcement also occurs for the tested to predicted shear stresses using NEN-EN 1992-1-1:2005 [8], although the

 doi:10.20944/preprints202206.0289.v1

increase is smaller than for ACI 318-19. On the other hand, the *fib* Model Code 2010 [9] shows consistency between shear-reinforced specimens and those without shear reinforcement. Nevertheless, this model tends to overestimate the shear resistance when evaluating shear-reinforced slabs.

All three models evaluated performed differently when evaluating internal, edge and corner slab column connections. Nevertheless, the Model Code 2010 [9] showed more consistency in terms of a relatively similar scatter and average tested to predicted values for all three cases. The ACI 318-19 [7] and the NEN-EN 1992-1-1:2005 [8] tend to get more conservative for edge and corner slab-column connections, as shown in Tables 3 and 4.

The Model Code 2010 [9] model shows more consistency between internal, edge, and corner slab-column connections in terms of average tested to predicted results, with relatively similar values of the COV for all the cases. However, this model could only be applied to 63% of the specimens in the database, given that it only works effectively when the slab effective depth and maximum aggregate size are close to common practice measures. For small scale slabs, the expressions from the *fib* Model Code are outside of their scope of application. In addition, the method can only be used when direct shear loads are applied to the slab-column connection.

As can be observed in Figure 18 and Table 5, the ACI 318-19 [7] assumption of a linear elastic model distribution leads to an underestimation of the real performance of the specimens. Replacing the shear stresses calculated assuming the linear stress distribution by the average values for the SCIA Engineer [23] FEM results in the comparison to the shear capacity from ACI 318-19 (see Table 5) results in smaller (i.e. less overly conservative) values for the tested to predicted shear. At the same time, the COV on the tested to predicted values increases, indicating that when using ACI 318-19, both the shear stress from the code provisions and the shear capacity should be used together.

As can be observed in Figure 19 and Table 6, the ACI 318-19 [7] assumption of a linear elastic model distribution does not hold up for finer calculations using the SCIA Engineer [23] FEM results. Despite the average value for the comparison between the shear capacities for ACI 318-19 [7] and SCIA Engineer [23] FEM results for the acting shear stress is relatively close to 1.0, the COV on these results is not acceptable (COV = 56.85). See Tables B4-B6.

3.3. Influence of parameters on tested to predicted punching capacities

Figure 20 shows the v_{test}/v_{pred} values as a function of the different parameters, studied in section 3.1, for the various codes with the objective of obtaining an insight in which codes over- or underestimate the various parameters.

Preprints (www.preprints.org) | NOT PEER-REVIEWED | Posted: 21 June 2022 doi:10.20944/preprints202206.0289.v1

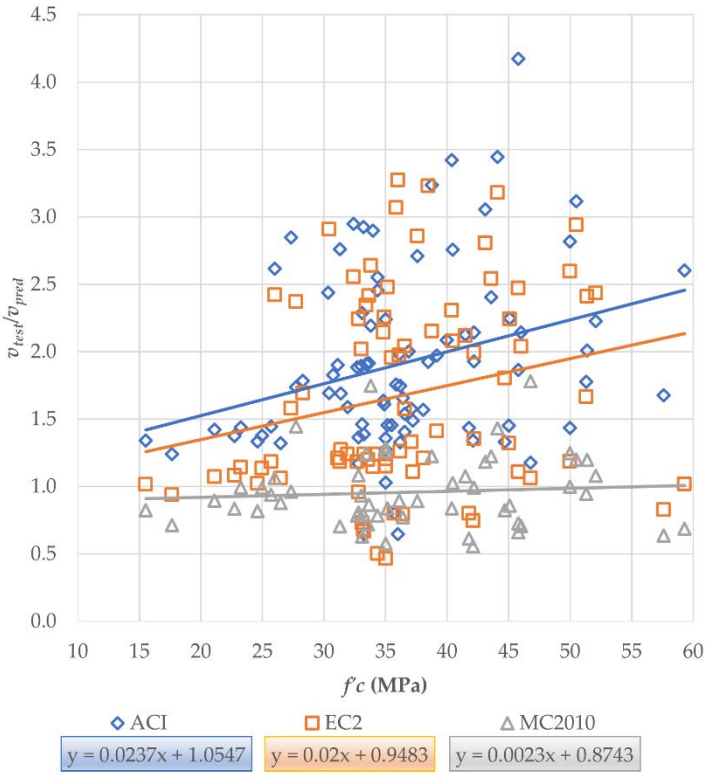

(a)

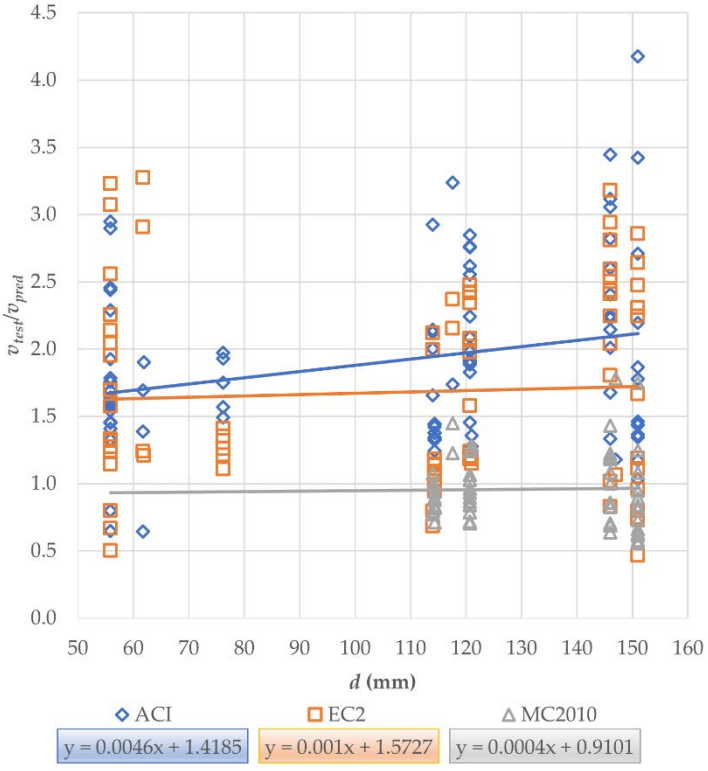

(b)

Preprints (www.preprints.org) | NOT PEER-REVIEWED | Posted: 21 June 2022 doi:10.20944/preprints202206.0289.v1

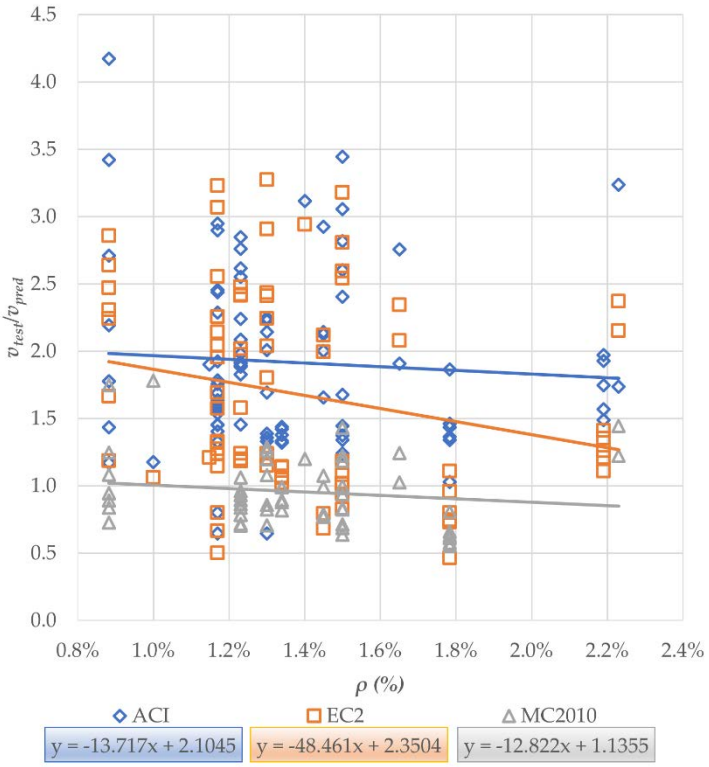

(c)

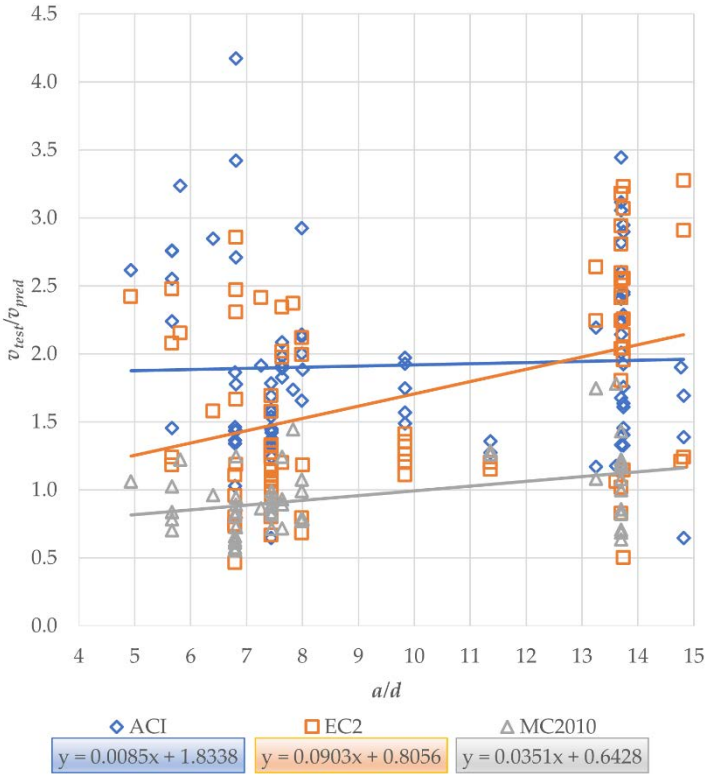

(d)

Figure 20. Parameters studied based on the comparison between experimental v_{test} and predicted shear capacities v_{pred} for 3 design methods from existing codes: (a)) concrete compressive strength f'_c ; (b) effective depth d; (c) longitudinal reinforcement ratio ρ; (d) shear span to depth ratio a/d.

 doi:10.20944/preprints202206.0289.v1

As can be observed in Figure 20a, ACI 318-19 [7] and NEN-EN 1992-1-1:2005 [8] tend to underestimate the influence of the compressive strength of the concrete f_c'. On the other hand, the *fib* Model Code correctly takes the influence of the concerte compressive strength into account.

When considering the influence of the effective depth d on the tested to predicted ratios (Figure 20b), we can see that NEN-EN 1992-1-1:2005 and the *fib* Model Code take the size effect correctly into account for the small specimens tested. ACI 318-19 has a trigger for the size effect at 254 mm, and thus for the small specimens tested, no influence of size is considered. Unexpectedly, we observe a small increase in the conservativism of ACI 318-19 as the effective depth increases.

As can be seen in Figure 20c, NEN-EN 1992-1-1:2005 [8] considers that the influence of the longitudinal reinforcement is larger than as observed in the experiments. The influence is taken into account more realistically in ACI 318-19 [7] and the *fib* Model Code 2010 [9]. As the specimens in the database contained large reinforcement ratios, experiments on slabs with lower reinforcement ratios are necessary to further study the effect of the reinforcement ratio on the tested to predicted ratios determined with the studied codes.

Figure 20d shows that for Model Code 2010 [9] and NEN-EN 1992-1-1:2005 [8] as the shear span to depth ratio a/d increases, the values of v_{test}/v_{pred} tend become more conservative. On the other hand, for ACI 318-19 [7] the values of v_{test}/v_{pred} tend to remain constant as the shear span to depth ratio increases.

4. Discussion

High strength concrete slabs are not included in the study due to the lack of experiments on high-strength concrete slab-column connections. Future studies may investigate the behavior of this type of slabs in comparison with the ones considered in this study. Ngo [25] presents a study on concentric experiments in high strength concrete slabs without shear reinforcement and concluded that the use of high strength concrete improves the punching shear resistance [26]. However, as aggregate interlock capacity decreases for higher strength concrete, further research on this topic is warranted.

Real scale slab-column experiments in punching shear are not commonly found in the literature. None of the entries in this database is considered as a realistic size slab as none of these has an effective depth over 200 mm. Since a size effect occurs in punching for concentric slab-column connections [27], experimental research on larger slabs under eccentric punching shear is necessary.

In most cases, the results found in the literature indicate that there is an important reduction of the punching capacity when unbalanced moments occur in the slab-column connection. Nevertheless, most experimental databases, and research focus on concentric punching shear. The code provisions are based on empirical equations that include the effect of eccentricities by different methods, such as critical perimeter reduction or increase of the applied shear stress, but a mechanics-based model that is practical enough to be implemented in the building codes is lacking. Mechanics-based models such as the Critical Shear Crack Theory used in the Model Code 2010 [9] are developed for the case of concentric punching shear and use simplified assumption for the extension to eccentric punching shear.

For this database, the empirical methods showed large scatter on the results of the tested to predicted capacities, represented by the high coefficients of variation. This observation may be explained by the fact that all methods under consideration were originally developed for concentric punching shear, and validated with concentric punching shear tests, and then extended to the use of eccentric punching shear.

 doi:10.20944/preprints202206.0289.v1

5. Conclusions

The lack of understanding regarding eccentric punching shear presents a practical problem because local forces typically control the slab's design. The transfer of unbalanced moments from the slab to the column causes an increase of the resulting shear stress. When this effect is not well-understood, it may lead to a punching failure of the slab-column connection and a possible collapse of the building. This study evaluates the available code provisions against 88 experimental results reported in the literature.

Analyzing the available experimental results from the database resulted in the following conclusions:

- All experiments are carried out in slabs under 200 mm depth. As such, the experiments cannot be used to evaluate the size effect in shear.
- There is a lack of experiments in eccentric punching shear.
- Most specimens have large reinforcement ratios to avoid a flexural failure before reaching the punching shear capacity of the slab.
- All specimens are cast using normal strength concrete.

The parametric studies led to the following observations:

- An analysis of the data showed that the shear stresses should be normalized to the square root of the concrete compressive strength. This ratio shows a smaller relation to concrete compressive strength than when shear stress is normalized to the cube root of the concrete compressive strength.
- The normalized shear strength increased as the reinforcement ratio increased. This influence was expected because a larger amount of reinforcement results in more dowel action, and thus a larger shear capacity.

From the comparison between the experimental shear capacities and the capacities predicted by the available codes, the following conclusion result:

- The closest to 1.0 average value for tested to predicted shear capacity is obtained with the Model Code 2010 [9] provisions, although the results err on the unsafe side (average of tested/predicted = 0.96).
- Evaluating all experiments, the coefficient of variation of the tested to predicted shear capacities is lower for the expressions of the Model Code 2010 [9], based on the Critical Shear Crack Theory, than for the empirical expressions from NEN-EN 1992-1-1:2005 [8] and ACI 318-19 [7].
- In general, the coefficient of variation of the tested to predicted shear capacities is lower for the experiments without shear reinforcement than for the experiments with shear reinforcement.
- The ACI 318-19 [7] results for tested to predicted shear capacity showed a smaller scatter for internal and corner slab-column connections than the results from NEN-EN 1992-1-1:2005 [8] and Model Code 2010 [9]. However, the ACI 318-19 [7] results for the tested to predicted shear stresses are not consistent throughout the various categories (internal, edge, and corner slab-column connections).
- The ACI 318-19 [7] the model has the lowest coefficient of variation on the tested to predicted shear stress for internal and corner slab-column connections, whereas the *fib* Model Code 2010 [9] has the smallest COV for the edge slab-column connections.
- The *fib* Model Code generally results in the best performance in the parameter studies of the tested to predicted ratios, indicating that this mechanics-based model takes the parameters into account in a correct manner.

From the comparison between the SCIA Engineer [23] FEM results and the predicted shear capacities for ACI 318-19 [7], the following conclusion result:

- Using a more refined calculation method to determine the acting shear stresses does not improve the results in terms of tested to predicted shear stresses when using the ACI 318-19 [7] shear capacities.

 doi:10.20944/preprints202206.0289.v1

- The ACI 318-19 [7] shear capacity should be combined with the method for determining the shear stress on the punching perimeter described in ACI 318-19 [7].
- Further research is necessary on capacity methods that can be combined with a linear finite element analysis.

A better understanding of eccentric punching shear and further experiments on deeper slabs and slabs with high-strength concrete are necessary to obtain safe designs, optimize the design of building floors, and develop better tools for the assessment of existing building slabs.

Author Contributions: conceptualization, EOLL.; methodology, DV and EOLL.; software, DV; validation, KG and EOLL.; formal analysis, DV.; investigation, DV and EOLL; resources, EOLL; data curation, DV and EOLL; writing—original draft preparation, DV and EOLL; writing—review and editing, KG; visualization, DV; supervision, EOLL; project administration, EOLL; funding acquisition, EOLL.

Funding: This research is part of the program of Collaboration Grants 2019 of Universidad San Francisco de Quito. The APC was funded by the open access initiative of Delft University of Technology.

Acknowledgments: The authors would like to thank the program of Collaboration Grants 2019 of Universidad San Francisco de Quito for the financial support.

Conflicts of Interest: The authors declare no conflict of interest.

List of notations

A_{sw}	area of the shear reinforcement for NEN-EN 1992-1-1:2005
A_v	area of the shear reinforcement in ACI 318-19
$C_{Rd,\,c}$	constant used for determining the shear capacity
E_s	modulus of elasticity of the steel
J_c	polar moment of inertia of the critical section
L_x	dimension of the slab
L_y	dimension of the slab
M_{Ed}	design moment
M_{mu}	model ultimate internal moment
M_u	factored moment applied on the slab
U_1	control perimeter for NEN-EN 1992-1-1:2005
U_1*	reduced critical control perimeter for NEN-EN 1992-1-1:2005
V_{Ed}	design shear strength
V_{Rd}	punching resistance for Model Code 2010
$V_{Rd,c}$	punching resistance provided by the concrete for Model Code 2010
$V_{Rd,s}$	punching resistance provided by the steel for Model Code 2010
V_u	factored shear applied on the slab
V_{mu}	model ultimate internal shear
W_{sup}	width of the support
W_1	plastic modulus of control perimeter for NEN-EN 1992-1-1:2005
a	shear span
a_v	clear shear span
b_0	control perimeter for Model Code 2010
$b_{0,int}$	critical perimeter inside the shear reinforced zone for CSCT
b_1	dimension of the critical perimeter for NEN-EN 1992-1-1:2005
$b_{1,MC}$	basic control perimeter for Model Code 2010
b_2	dimension of the critical perimeter for Model Code 2010
b_o	perimeter of the critical perimeter for ACI 318-19
b_u	diameter of the circle with the same area as the region inside $b_{1,\,MC}$
b_y	dimension on the critical perimeter U_1

b_z	dimension on the critical perimeter U_1
c	distance to the centroid of the critical perimeter
c_1	dimension of the column
c_2	dimension of the column
d	average effective depth of the slab
d_g	maximum aggregate size
d_v	average effective depth of the slab for Model Code 2010
e	eccentricity M/V
e_{par}	eccentricity parallel to the edge of the slab
e_u	eccentricity of the resultant forces
e_y	eccentricity caused by a moment acting on the y- axis
e_z	eccentricity caused by a moment acting on the x- axis
f_{bd}	bond strength
f_c	compressive strength of the concrete for ACI 318-19
f_{ck}	compressive strength of the concrete for Model Code 2010
f_{ct}	tensile strength of the concrete
f_{yt}	yield strength of the reinforcement
f_{ywd}	design yield strength of the shear reinforcement
$f_{ywd,ef}$	effective design strength of shear reinforcement
h	depth of the slab
k	size effect factor
k_c	column size effect factor
k_{dg}	coefficient of aggregate size
k_e	coefficient of eccentricity
k_ψ	coefficient of rotation
m_{rd}	average flexural strength per unit length in the support strip
m_{sd}	average moment per unit length for calculation flexural reinforcement in the support strip
r_s	distance from column axis to line of contraflexure of the radial bending moments
m_{xD}	model design moment on the x- axis.
m_{yD}	model design moment on the y- axis
s_r	radial spacing of the reinforcement
v_c	punching resistance provided by the concrete for ACI 318-19
v_{Ed}	design shear stress
v_n	nominal shear strength for ACI 318-19
$v_{Rd,\,c}$	shear resistance provided by the concrete
v_{Rd}	shear resistance for Model Code 2010
$v_{Rd,cs}$	shear resistance for NEN-EN 1992-1-1:2005
$v_{Rd\,s}$	shear resistance provided by the steel
v_s	punching resistance provided by the steel reinforcement for ACI 318-19
v_u	maximum shear stress for ACI 318-19
v_{pred}	shear capacity predicted for al the models
v_{FEM}	maximum shear stress from the FEM model
γ_f	fraction of the unbalanced moment transmitted by flexure
γ_v	fraction of the unbalanced moment transmitted by shear
α	angle between shear reinforcement and horizontal plane of the slab
α_s	constant used for determining shear capacity according to ACI 318-19
β	column sizes relation factor according to ACI 318-19
β_{EC}	enhancement factor for eccentric shear for NEN-EN 1992-1-1:2005
ρ_l	longitudinal steel reinforcement ratio
ρ_v	shear steel reinforcement ratio
σ_{swd}	shear reinforcement stress
ϕ_w	shear reinforcement diameter

Preprints (www.preprints.org) | NOT PEER-REVIEWED | Posted: 21 June 2022 doi:10.20944/preprints202206.0289.v1

ψ rotation of the slab

Appendix A

Table A1. Internal slab-column connections – Slab geometry

Name	L_x (mm)	L_x (mm)	c_1 (mm)	c_2 (mm)	h (mm)	d (mm)	a (mm)	a_v (mm)
Narayani [16]								
L1	2285	2285	305	305	178	151	1026	874
L3	2285	2285	305	305	178	151	1026	875
L4	2285	2285	305	305	178	151	1026	876
L5	2285	2285	305	305	178	151	1026	877
L6	2285	2285	305	305	178	151	1026	878
L10	2285	2285	305	305	178	151	1026	879
Krüger [2]								
P16A	3000	3000	300	300	150	121	1375	880
P30A	3000	3000	300	300	150	121	1375	881
Moe [10]								
M2A	1829	1829	305	305	152	114	851	882
M4A	1829	1829	305	305	152	114	851	883
M2	1829	1829	305	305	152	114	851	884
M3	1829	1829	305	305	152	114	851	885
M6	1829	1829	254	254	152	114	851	886
M7	1829	1829	254	254	152	114	851	887
M8	1829	1829	254	254	152	114	851	888
M9	1829	1829	254	254	152	114	851	889
M10	1829	1829	254	254	152	114	851	890
Anis [18]								
B.3	1524	1524	203	203	102	76	749	891
B.4	1524	1524	203	203	102	76	749	892
B.5	1524	1524	203	203	102	76	749	893
B.6	1524	1524	203	203	102	76	749	894
B.7	1524	1524	203	203	102	76	749	895
Stamenkovic [20]								
C/I/1	914	914	127	127	76	56	416	896
C/I/2	914	914	127	127	76	56	416	897
C/I/3	914	914	127	127	76	56	416	898
C/I/4	914	914	127	127	76	56	416	899
C/Ir/1	914	914	152	76	76	56	416	900
C/Ir/2	914	914	152	76	76	56	416	901
C/Ir/3	914	914	152	76	76	56	416	902
C/Ir/4	914	914	152	76	76	56	416	903
Hanson & Hanson [19]								
A12	2134	1219	152	152	76	62	914	904
B16	2134	1219	152	305	76	62	914	905

Preprints (www.preprints.org) | NOT PEER-REVIEWED | Posted: 21 June 2022 doi:10.20944/preprints202206.0289.v1

C17	2134	1219	305	152	76	62	914	906

Table A2. Internal slab-column connections – Material properties

Name	ρ (%)	f_y (MPa)	E_s (GPa)	f_c (MPa)	age (days)	f_{ct} (MPa)	d_g (mm)
Narayani [16]							
L1	1.78%	398	188	32.80	28	2.70	19.00
L3	1.78%	398	188	33.10	28	2.66	19.00
L4	1.78%	398	188	45.80	28	3.45	19.00
L5	1.78%	398	188	35.00	28	2.98	19.00
L6	1.78%	398	188	42.10	28	3.07	19.00
L10	1.78%	398	188	41.80	28	2.47	19.00
Krüger [2]							
P16A	1.30%	480	200	35.00	28	4.50	16.00
P30A	1.30%	480	200	35.00	28	4.50	16.00
Moe [10]							
M2A	1.50%	481	196	15.51	25	2.99	38.10
M4A	1.50%	481	196	17.65	23	3.19	38.10
M2	1.50%	481	196	25.72	22	3.85	38.10
M3	1.50%	481	196	22.72	20	3.62	38.10
M6	1.34%	328	196	26.48	26	3.91	38.10
M7	1.34%	328	196	24.96	24	3.80	38.10
M8	1.34%	328	196	24.61	24	3.77	38.10
M9	1.34%	328	196	23.24	22	3.66	38.10
M10	1.34%	328	196	21.10	25	3.49	38.10
Anis [18]							
B.3	2.19%	331	205	38.06	28	4.69	9.53
B.4	2.19%	331	205	37.23	28	4.64	9.53
B.5	2.19%	331	205	36.20	28	4.57	9.53
B.6	2.19%	331	205	39.16	28	4.76	9.53
B.7	2.19%	331	205	42.20	28	4.94	9.53
Stamenkovic [20]							
C/I/1	1.17%	434	200	45.02	7	5.10	9.53
C/I/2	1.17%	434	200	37.09	7	4.63	9.53
C/I/3	1.17%	434	200	31.92	7	4.29	9.53
C/I/4	1.17%	434	200	31.37	7	4.26	9.53
C/Ir/1	1.17%	414	200	28.27	7	4.04	9.53
C/Ir/2	1.17%	414	200	36.54	7	4.59	9.53
C/Ir/3	1.17%	414	200	35.71	7	4.54	9.53
C/Ir/4	1.17%	414	200	33.23	7	4.38	9.53
Hanson & Hanson [19]							
A12	1.30%	372	200	33.23	28	4.38	9.53
B16	1.30%	341	200	30.41	28	4.19	9.53
C17	1.30%	341	200	35.99	28	4.56	9.53

Preprints (www.preprints.org) | NOT PEER-REVIEWED | Posted: 21 June 2022 doi:10.20944/preprints202206.0289.v1

Table A3. Edge slab-column connections – Slab geometry

Name	L_x (mm)	L_x (mm)	c_1 (mm)	c_2 (mm)	h (mm)	d (mm)	a (mm)	a_v (mm)
Albuquerque [14]								
L1	2350	1700	300	300	180	147	2000	907
L2	2350	1700	300	300	180	146	2000	908
L3	2350	1700	300	300	180	146	2000	909
L4	2350	1700	300	300	180	146	2000	910
L5	2350	1700	300	300	180	146	2000	911
L6	2350	1700	300	300	180	146	2000	912
L7	2350	1700	300	300	180	146	2000	913
L8	2350	1700	300	300	180	146	2000	914
L9	2350	1700	300	300	180	146	2000	915
L10	2350	1700	300	300	180	146	2000	916
L11	2350	1700	300	300	180	146	2000	917
L12	2350	1700	300	300	180	146	2000	918
L13	2350	1700	300	300	180	146	2000	919
Narayani [16]								
ES1	1295	2285	305	305	178	151	2000	920
ES2	1295	2285	305	305	178	151	2000	921
ES3	1295	2285	305	305	178	151	1029	922
ES4	1295	2285	305	305	178	151	1029	923
ES5	1295	2285	305	305	178	151	1029	924
ES6	1295	2285	305	305	178	151	1029	925
ES7	1295	2285	305	305	178	151	1029	926
Zaghlool [17]								
Z - IV (1)	965	1829	178	178	152	121	773	927
Z - V (1)	965	1829	267	267	152	121	684	928
Z - V (2)	965	1829	267	267	152	121	684	929
Z - V (3)	965	1829	267	267	152	118	684	930
Z - V (4)	965	1829	267	267	152	121	684	931
Z - V (5)	965	1829	267	267	152	121	684	932
Z - V (6)	965	1829	267	267	152	121	684	933
Z - VI (1)	965	1829	356	356	152	121	595	934
Stamenkovic [20]								
M(T)/E/1	914	914	127	127	76	56	768	935
M(T)/E/2	914	914	127	127	76	56	768	936
C(T)/E/1	914	914	127	127	76	56	768	937
C(T)/E/2	914	914	127	127	76	56	768	938
C(T)/E/3	914	914	127	127	76	56	768	939
C(T)/E/4	914	914	127	127	76	56	768	940
M(II)/E/1	914	914	127	127	76	56	768	941
C(II)/E/1	914	914	127	127	76	56	768	942
C(II)/E/2	914	914	127	127	76	56	768	943

Preprints (www.preprints.org) | NOT PEER-REVIEWED | Posted: 21 June 2022 doi:10.20944/preprints202206.0289.v1

C(II)/E/3	914	914	127	127	76	56	768	944
C(II)/E/4	914	914	127	127	76	56	768	945
V/E/1	914	914	127	127	76	56	768	946
Hanson & Hanson [19]								
D15	1143	1219	152	152	76	62	914	946.5

Table A4. Edge slab-column connections – Material properties

Name	ρ (%)	f_y (MPa)	E_s (GPa)	f_c (MPa)	age (days)	f_{ct} (MPa)	d_g (mm)
Albuquerque [14]							
L1	1.00%	558	192	46.80	28	3.40	9.50
L2	1.30%	558	192	44.70	28	3.00	9.50
L3	1.30%	558	192	45.10	28	3.10	9.50
L4	1.30%	558	192	46.00	28	3.30	9.50
L5	1.30%	558	192	51.40	28	4.10	9.50
L6	1.30%	558	192	52.10	28	4.30	9.50
L7	1.50%	558	192	50.00	28	3.70	9.50
L8	1.40%	558	192	50.50	28	3.90	9.50
L9	1.50%	558	192	57.60	28	3.20	9.50
L10	1.50%	558	192	59.30	28	3.60	9.50
L11	1.50%	558	192	43.10	28	3.10	9.50
L12	1.50%	558	192	43.60	28	3.30	9.50
L13	1.50%	558	192	44.10	28	3.40	9.50
Narayani [16]							
ES1	0.88%	398	188	33.80	28	2.70	19.00
ES2	0.88%	398	188	32.80	28	2.70	19.00
ES3	0.88%	398	188	51.30	28	3.10	19.00
ES4	0.88%	398	188	50.00	28	3.31	19.00
ES5	0.88%	398	188	37.60	28	2.63	19.00
ES6	0.88%	398	188	40.40	28	2.23	19.00
ES7	0.88%	398	188	45.80	28	3.38	19.00
Zaghlool [17]							
Z - IV (1)	1.23%	476	200	27.34	28	2.99	19.05
Z - V (1)	1.23%	474	200	34.34	28	3.52	19.05
Z - V (2)	1.65%	474	200	40.47	28	3.61	19.05
Z - V (3)	2.23%	475	200	38.75	28	3.79	19.05
Z - V (4)	1.23%	437	200	35.03	28	4.10	19.05
Z - V (5)	1.23%	476	200	35.16	28	3.58	19.05
Z - V (6)	1.23%	476	200	31.30	28	3.63	19.05
Z - VI (1)	1.23%	476	200	25.99	28	2.83	19.05
Stamenkovic [20]							
M(T)/E/1	1.17%	496	200	30.34	7	4.19	9.53
M(T)/E/2	1.17%	496	200	33.09	7	4.37	9.53
C(T)/E/1	1.17%	496	200	38.47	7	4.71	9.53

Preprints (www.preprints.org) | NOT PEER-REVIEWED | Posted: 21 June 2022 doi:10.20944/preprints202206.0289.v1

C(T)/E/2	1.17%	496	200	32.41	7	4.33	9.53
C(T)/E/3	1.17%	496	200	33.99	7	4.43	9.53
C(T)/E/4	1.17%	496	200	34.34	7	4.45	9.53
M(II)/E/1	1.17%	448	200	36.20	7	4.57	9.53
C(II)/E/1	1.17%	448	200	34.82	7	4.48	9.53
C(II)/E/2	1.17%	448	200	35.51	7	4.53	9.53
C(II)/E/3	1.17%	414	200	34.89	7	4.49	9.53
C(II)/E/4	1.17%	448	200	36.54	7	4.59	9.53
V/E/1	1.17%	496	200	35.85	7	4.55	9.53
Hanson & Hanson [19]							
D15	1.15%	365	200	31.10	28	4.24	9.53

Table A5. Corner slab-column connections – Slab geometry

Name	L_x (mm)	L_x (mm)	c_1 (mm)	c_2 (mm)	h (mm)	d (mm)	a (mm)	a_v (mm)
Zaghlool [17]								
Z - I (1)	1067	1067	178	178	152	121	965	948
Z - II (1)	1067	1067	267	267	152	121	921	949
Z - II (2)	1067	1067	267	267	152	121	921	950
Z - II (3)	1067	1067	267	267	152	118	921	951
Z - II (4)	1067	1067	267	267	152	121	921	952
Z - II (6)	1067	1067	267	267	152	121	921	953
Z - II (7)	1067	1067	267	267	152	121	921	954
Z - II (8)	1067	1067	267	267	152	121	921	955
Z - III (1)	1067	1067	356	356	152	121	876	956
Hammill & Ghali [15]								
NH1	1075	1075	250	250	150	114	910	957
NH2	1075	1075	250	250	150	114	910	958
NH3	1075	1075	250	250	150	114	910	959
NH4	1075	1075	250	250	150	114	910	960
NH5	1075	1075	250	250	150	114	910	961

Table A6. Corner slab column connections – Materials description

Name	ρ (%)	f_y (MPa)	E_s (GPa)	f_c (MPa)	age (days)	f_{ct} (MPa)	d_g (mm)
Zaghlool [17]							
Z - I (1)	1.23%	379	207	32.68	28	3.83	19.05
Z - II (1)	1.23%	389	207	33.03	28	3.63	19.05
Z - II (2)	1.65%	405	207	33.44	28	3.83	19.05
Z - II (3)	2.23%	451	207	27.72	28	3.18	19.05
Z - II (4)	1.23%	389	207	30.75	28	3.36	19.05
Z - II (6)	1.23%	381	207	33.58	28	3.04	19.05
Z - II (7)	1.23%	382	207	39.99	28	3.81	19.05
Z - II (8)	1.23%	382	207	36.10	28	3.50	19.05
Z - III (1)	1.23%	379	207	33.65	28	3.94	19.05

Preprints (www.preprints.org) | NOT PEER-REVIEWED | Posted: 21 June 2022 doi:10.20944/preprints202206.0289.v1

Hammill & Ghali [15]							
NH1	1.45%	440	200	41.50	28	4.90	9.50
NH2	1.45%	440	200	42.20	28	4.94	9.50
NH3	1.45%	440	200	36.40	28	4.59	9.50
NH4	1.45%	440	200	36.90	28	4.62	9.50
NH5	1.45%	440	200	33.20	28	4.38	9.50

Table A7. Database, shear reinforcement

Name	**Type**	f_y **(MPa)**	E_s **(GPa)**	Φ_w **(mm)**	s **(mm)**
Interior slab column connections					
Narayani [16]					
L3	Shear Hats	309	207	9.5	90
L4	Shear Hats	238	207	6.5	90
L5	Shear Hats	355	207	13	90
L6	Shear Hats	355	207	8	90
L10	Shear Hats	355	207	8	90
Edge slab column connections					
Albuquerque [14]					
L9	Shear Heads	587	188	8	100
L10	Shear Heads	587	188	8	100
Narayani [16]					
ES3	Stir-rups	238	207	6.5	70
ES4	Stir-rups	309	207	9.5	70
ES6	Stir-rups	238	207	6.5	70
ES7	Stir-rups	238	207	6.5	70
Corner slab column connections					
Hammill & Ghali [15]					
NH3	Shear Heads	440	200	6	57
NH5	Shear Heads	440	200	6	85

Figure 12 illustrates the 'Shear Hats' type of shear reinforcement

Preprints (www.preprints.org) | NOT PEER-REVIEWED | Posted: 21 June 2022 doi:10.20944/preprints202206.0289.v1

Appendix B

Table B1. Internal slab-column connections – Tested to Predicted shear capacity

Name	ACI [7]			EC2 [8]			MC 2010 [9]		
	Test (MPa)	Pred (MPa)	Test/Pred	Test (MPa)	Pred (MPa)	Test/Pred	Test (MPa)	Pred (MPa)	Test/Pred
Narayani [16]									
L1	2.58	1.89	1.37	1.34	1.40	0.96	2.49	3.08	0.81
L3	3.23	2.21	1.46	1.49	2.04	0.73	1.97	3.12	0.63
L4	3.67	1.97	1.87	1.70	1.53	1.11	2.24	3.40	0.66
L5	3.23	3.13	1.03	1.49	3.21	0.47	1.97	3.42	0.58
L6	3.02	2.25	1.34	1.46	1.95	0.75	1.92	3.43	0.56
L10	3.22	2.24	1.44	1.56	1.95	0.80	2.05	3.33	0.61
Krüger [2]									
P16A	2.49	1.95	1.28	1.48	1.29	1.15	2.52	2.00	1.26
P30A	2.65	1.95	1.36	1.55	1.29	1.20	2.63	2.04	1.29
Moe [10]									
M2A	1.74	1.30	1.34	1.04	1.03	1.02	1.73	2.10	0.82
M4A	1.72	1.39	1.24	1.01	1.07	0.94	1.65	2.31	0.71
M2	2.42	1.67	1.45	1.44	1.22	1.18	2.38	2.53	0.94
M3	2.17	1.57	1.38	1.27	1.17	1.08	2.08	2.49	0.84
M6	2.25	1.70	1.32	1.26	1.18	1.06	2.24	2.55	0.88
M7	2.27	1.65	1.38	1.32	1.16	1.14	2.35	2.38	0.99
M8	2.19	1.64	1.34	1.18	1.15	1.02	2.10	2.57	0.82
M9	2.29	1.59	1.44	1.30	1.13	1.15	2.31	2.33	0.99
M10	2.16	1.52	1.42	1.18	1.10	1.07	2.10	2.34	0.90
Anis [18]									
B.3	3.19	2.04	1.57	1.91	1.57	1.21	-	-	-
B.4	3.00	2.01	1.49	1.73	1.56	1.11	-	-	-
B.5	3.47	1.99	1.75	1.95	1.55	1.26	-	-	-
B.6	4.07	2.07	1.97	2.24	1.59	1.41	-	-	-
B.7	4.13	2.14	1.93	2.20	1.63	1.35	-	-	-
Stamenkovic [20]									
C/I/1	3.21	2.21	1.45	1.78	1.35	1.32	-	-	-
C/I/2	3.17	2.01	1.58	1.69	1.27	1.33	-	-	-
C/I/3	2.97	1.86	1.59	1.50	1.20	1.24	-	-	-
C/I/4	3.12	1.85	1.69	1.52	1.20	1.27	-	-	-
C/Ir/1	3.13	1.75	1.78	1.96	1.16	1.70	-	-	-
C/Ir/2	3.07	1.99	1.54	1.99	1.26	1.58	-	-	-
C/Ir/3	1.58	1.97	0.80	1.00	1.25	0.80	-	-	-
C/Ir/4	1.23	1.90	0.65	0.81	1.22	0.67	-	-	-
Hanson & Hanson [19]									
A12	2.64	1.90	1.39	1.57	1.26	1.24	-	-	-
B16	3.18	1.87	1.69	3.57	1.23	2.91	-	-	-
C17	1.32	2.04	0.65	4.25	1.30	3.27	-	-	-

Preprints (www.preprints.org) | NOT PEER-REVIEWED | Posted: 21 June 2022 doi:10.20944/preprints202206.0289.v1

Table B2. Edge slab-column connections – Tested to Predicted shear capacity

Name	ACI [7]			EC2 [8]			MC 2010 [9]		
	Test (MPa)	Pred (MPa)	Test/Pred	Test (MPa)	Pred (MPa)	Test/Pred	Test (MPa)	Pred (MPa)	Test/Pred
Albuquerque [14]									
L1	2.66	2.26	1.18	1.38	1.30	1.06	3.07	1.72	1.78
L2	2.94	2.21	1.33	2.52	1.39	1.81	1.91	2.31	0.83
L3	4.98	2.22	2.25	3.14	1.40	2.24	2.57	2.99	0.86
L4	4.80	2.24	2.14	2.87	1.41	2.04	2.39	3.38	0.71
L5	4.75	2.37	2.01	3.52	1.46	2.41	2.76	2.31	1.20
L6	5.31	2.38	2.23	3.58	1.47	2.44	2.88	2.66	1.08
L7	6.58	2.33	2.82	3.94	1.52	2.60	3.28	3.27	1.00
L8	7.31	2.35	3.12	4.38	1.49	2.94	3.64	3.03	1.20
L9	4.57	2.72	1.68	2.40	2.90	0.83	1.34	2.10	0.64
L10	7.16	2.75	2.60	2.96	2.91	1.02	1.75	2.55	0.69
L11	6.62	2.17	3.06	4.06	1.44	2.81	3.35	2.83	1.18
L12	5.24	2.18	2.41	3.69	1.45	2.54	2.93	2.40	1.22
L13	7.55	2.19	3.45	4.63	1.46	3.18	3.82	2.67	1.43
Narayani [16]									
ES1	4.21	1.92	2.19	2.95	1.12	2.64	3.96	2.27	1.75
ES2	2.21	1.89	1.17	2.48	1.11	2.24	2.20	2.03	1.08
ES3	2.86	1.61	1.78	2.46	1.48	1.67	2.01	2.12	0.95
ES4	3.29	2.29	1.44	2.83	2.38	1.19	2.31	1.85	1.25
ES5	5.49	2.02	2.71	3.31	1.16	2.86	2.41	2.70	0.89
ES6	5.04	1.47	3.42	3.24	1.40	2.31	1.86	2.22	0.84
ES7	6.44	1.54	4.18	3.56	1.44	2.47	2.00	2.74	0.73
Zaghlool [17]									
Z - IV (1)	4.91	1.73	2.85	1.84	1.16	1.58	2.73	2.84	0.96
Z - V (1)	4.94	1.93	2.55	1.56	1.25	1.24	2.33	2.97	0.78
Z - V (2)	5.79	2.10	2.76	3.04	1.46	2.08	3.47	3.38	1.03
Z - V (3)	6.65	2.05	3.24	3.43	1.59	2.15	3.93	3.21	1.22
Z - V (4)	4.38	1.95	2.24						
Z - V (5)	2.85	1.96	1.46	3.13	1.26	2.48	2.34	2.79	0.84
Z - V (6)	5.10	1.85	2.76	1.44	1.22	1.19	2.30	3.27	0.70
Z - VI (1)	4.40	1.68	2.62	2.77	1.14	2.42	2.75	2.59	1.06
Stamenkovic [20]									
M(T)/E/1	4.43	1.82	2.44	-	-	-	-	-	-
M(T)/E/2	4.35	1.90	2.29	-	-	-	-	-	-
C(T)/E/1	3.94	2.05	1.92	4.14	1.28	3.23	-	-	-
C(T)/E/2	5.54	1.88	2.95	3.09	1.21	2.56	-	-	-
C(T)/E/3	5.58	1.92	2.90	1.41	1.23	1.15	-	-	-
C(T)/E/4	4.75	1.93	2.46	0.62	1.23	0.50	-	-	-
M(II)/E/1	2.64	1.99	1.33	-	-	-	-	-	-
C(II)/E/1	3.19	1.95	1.64	2.65	1.24	2.14	-	-	-

Preprints (www.preprints.org) | NOT PEER-REVIEWED | Posted: 21 June 2022 doi:10.20944/preprints202206.0289.v1

C(II)/E/2	2.86	1.97	1.46	2.44	1.25	1.95	-	-	-
C(II)/E/3	3.14	1.95	1.61	2.80	1.24	2.26	-	-	-
C(II)/E/4	2.81	1.99	1.41	2.57	1.26	2.04	-	-	-
V/E/1	3.47	1.98	1.76	3.84	1.25	3.07	-	-	-
Hanson & Hanson [19]									
D15	3.50	1.84	1.90	1.44	1.19	1.21	-	-	-

Table B3. Corner slab-column connections – Tested to Predicted shear capacity

Name	ACI [7]			EC2 [8]			MC 2010 [9]		
	Test (MPa)	Pred (MPa)	Test/Pred	Test (MPa)	Pred (MPa)	Test/Pred	Test (MPa)	Pred (MPa)	Test/Pred
Zaghlool [17]									
Z - I (1)	2.89	1.89	1.89	1.46	1.23	1.18	2.69	3.43	0.78
Z - II (1)	3.38	1.90	1.90	2.50	1.24	2.02	3.20	3.43	0.93
Z - II (2)	4.62	1.91	1.91	3.21	1.37	2.34	4.26	3.42	1.24
Z - II (3)	5.13	1.74	1.74	3.38	1.42	2.37	4.57	3.16	1.45
Z - II (4)	2.00	1.83	1.83	-	-	-	-	-	-
Z - II (6)	3.14	1.91	1.91	1.49	1.24	1.20	2.48	3.46	0.72
Z - II (7)	2.04	2.09	2.09	-	-	-	-	-	-
Z - II (8)	3.39	1.98	1.98	2.52	1.27	1.98	3.22	3.59	0.90
Z - III (1)	3.06	1.91	1.91	3.01	1.25	2.42	3.01	3.47	0.87
Hammill & Ghali [15]									
NH1	4.43	2.13	2.13	2.99	1.41	2.12	4.04	3.76	1.08
NH2	4.15	2.14	2.14	2.83	1.42	2.00	3.80	3.83	0.99
NH3	4.28	2.58	1.66	1.89	2.38	0.80	2.88	3.72	0.77
NH4	2.79	2.00	2.00	-	-	-	-	-	-
NH5	5.69	1.95	2.93	1.30	1.90	0.69	2.58	3.26	0.79

Table B4. Internal slab-column connections – SCIA (FEM) [23] results to tested and predicted shear stress, Eq. (1), and capacity for ACI [7]

ACI [7]		SCIA (FEM) [23]		
Pred (MPa)	Tested (MPa)	Result (MPa)	FEM Result/Pred	Tested/ FEM Result
Narayani [16]				
1.89	2.58	4.24	2.24	1.15
2.21	3.23	2.48	1.13	2.87
1.97	3.67	2.83	1.44	2.56
3.13	3.23	2.48	0.79	4.07

Preprints (www.preprints.org) | NOT PEER-REVIEWED | Posted: 21 June 2022 doi:10.20944/preprints202206.0289.v1

2.25	3.02	2.33	1.03	2.92
2.24	3.22	2.48	1.11	2.91
		Krüger [2]		
1.95	2.49	2.90	1.49	1.68
1.95	2.65	2.96	1.51	1.75
		Moe [10]		
1.30	1.74	2.54	1.95	0.89
1.39	1.72	2.89	2.09	0.83
1.67	2.42	3.58	2.14	1.13
1.57	2.17	3.51	2.23	0.97
1.70	2.25	3.23	1.90	1.18
1.65	2.27	2.84	1.72	1.32
1.64	2.19	3.66	2.24	0.98
1.59	2.29	3.15	1.98	1.16
1.52	2.16	3.42	2.26	0.96
		Anis [18]		
2.04	3.19	3.80	1.87	1.71
2.01	3.00	3.28	1.63	1.84
1.99	3.47	3.77	1.90	1.83
2.07	4.07	4.47	2.17	1.88
2.14	4.13	4.94	2.31	1.79
		Stamenkovic [20]		
2.21	3.21	4.02	1.81	1.77
2.01	3.17	4.57	2.27	1.39
1.86	2.97	3.86	2.07	1.43
1.85	3.12	4.11	2.23	1.40
1.75	3.13	3.29	1.87	1.67
1.99	3.07	3.42	1.71	1.79
1.97	1.58	1.69	0.86	1.84
1.90	1.23	1.42	0.75	1.65
		Hanson & Hanson [19]		
1.90	2.64	3.40	1.79	1.48
1.87	3.18	4.53	2.42	1.32
2.04	1.32	2.70	1.33	0.99

Table B5. Edge slab-column connections – SCIA (FEM) [23] results to tested and predicted shear stress, Eq. (1), and capacity for ACI [7]

ACI [7]		**SCIA (FEM) [23]**		
Pred (MPa)	Tested (MPa)	Result (MPa)	FEM Result/Pred	Tested/ FEM Result
		Albuquerque [14]		
2.26	2.66	2.59	1.15	2.32
2.21	2.94	2.50	1.13	2.60
2.22	4.98	2.92	1.32	3.78
2.24	4.80	2.70	1.21	3.97

 doi:10.20944/preprints202206.0289.v1

2.37	4.75	3.33	1.41	3.38
2.38	5.31	3.33	1.40	3.80
2.33	6.58	3.67	1.57	4.19
2.35	7.31	4.07	1.74	4.21
2.72	4.57	2.59	0.95	4.80
2.75	7.16	2.77	1.01	7.10
2.17	6.62	3.77	1.74	3.80
2.18	5.24	3.46	1.59	3.30
2.19	7.55	4.28	1.95	3.87
		Narayani [16]		
1.92	4.21	2.68	1.40	3.01
1.89	2.21	2.23	1.18	1.88
1.61	2.86	1.37	0.85	3.38
2.29	3.29	1.56	0.68	4.83
2.02	5.49	3.01	1.49	3.68
1.47	5.04	1.61	1.09	4.61
1.54	6.44	2.02	1.31	4.92
		Zaghlool [17]		
1.73	4.91	1.77	1.03	4.78
1.93	4.94	1.87	0.97	5.11
2.10	5.79	2.10	1.00	5.80
2.05	6.65	3.78	1.84	3.61
1.95	4.38	1.21	0.62	7.08
1.96	2.85	2.81	1.43	1.99
1.85	5.10	1.63	0.88	5.76
1.68	4.40	4.64	2.76	1.60
		Stamenkovic [20]		
1.82	4.43	3.69	2.03	2.18
1.90	4.35	3.62	1.91	2.28
2.05	3.94	3.13	1.53	2.58
1.88	5.54	4.29	2.28	2.43
1.92	5.58	4.50	2.34	2.38
1.93	4.75	3.89	2.01	2.36
1.99	2.64	3.24	1.63	1.61
1.95	3.19	6.69	3.44	0.93
1.97	2.86	5.63	2.86	1.00
1.95	3.14	5.28	2.71	1.16
1.99	2.81	4.23	2.12	1.32
1.98	3.47	3.87	1.96	1.78
		Hanson & Hanson [19]		
1.84	3.50	1.67	0.91	3.86

Table B6. Corner slab-column connections – SCIA (FEM) [23] results to tested and predicted shear stress, Eq. (1), and capacity for ACI [7]

ACI [7]		**SCIA (FEM) [23]**		
Pred (MPa)	Tested (MPa)	Result (MPa)	FEM Result/Pred	Tested/ FEM Result
		Zaghlool [17]		
1.89	2.89	1.84	0.97	2.96
1.90	3.38	3.35	1.77	1.91
1.91	4.62	3.86	2.03	2.28
1.74	5.13	4.17	2.40	2.14
1.83	2.00	4.02	2.20	0.91
1.91	3.14	2.19	1.15	2.74
2.09	2.04	4.12	1.97	1.04
1.98	3.39	3.42	1.72	1.97
1.91	3.06	4.47	2.33	1.31
		Hammill & Ghali [15]		
2.13	4.43	3.59	1.69	2.63
2.14	4.15	1.39	0.65	6.40
2.58	4.28	7.72	2.99	1.43
2.00	2.79	5.36	2.67	1.04
1.95	5.69	8.91	4.58	1.24

References

[1] J. Wight and J. MacGregor, *Analysis, and Design. In Reinforced Concrete Mechanics & Design*, 6th ed., vol. 1. London: Pearson, 2010.

[2] G. Krüger, "Résistance au poinçonnement excentré des planchers-dalles," *EPFL*, 1999.

[3] A. Muttoni, M. Fernández Ruiz, and J. T. Simões, "The theoretical principles of the critical shear crack theory for punching shear failures and derivation of consistent closed-form design expressions," *Structural Concrete*, vol. 19, no. 1, pp. 174–190, Feb. 2018, doi: 10.1002/suco.201700088.

[4] Y. Mirzaei, "Post punching behaviour of reinforced concrete slab-column connections," *7th International FIB PhD Symposium*, 2008.

[5] S. Kinnunen and Henrik Nylander, "Punching of concrete slabs without shear reinforcement," *Elander*, vol. 158, p. 112, 1960.

[6] A. Muttoni and M. F. Ruiz, "The levels-of-approximation approach in MC 2010: application to punching shear provisions," *Structural Concrete*, vol. 13, no. 1, pp. 32–41, Mar. 2012, doi: 10.1002/suco.201100032.

[7] ACI Committee 318, *ACI CODE-318-19: Building Code Requirements for Structural Concrete and Commentary*. Farmington Hills: American Concrete Institute, 2019.

[8] European Committee for Standardization and British Standards Institution, *Eurocode 2: design of concrete structures*. London: British Standards Institution, 2004.

[9] Walraven *et al.*, *fib Bulletin 55. Model Code 2010 First complete draft Volume 1*. fib. The International Federation for Structural Concrete, 2010. doi: 10.35789/fib.BULL.0056.

[10] J. Moe, "Shearing Strength of Reinforced Concrete Slabs and Footings under Concentrated Loads," *Development Department Bulletin D47*, Apr. 1961.

[11] ACI-ASCE Committee 426, "The Shear Strength of Reinforced Concrete Members," Chapter 5, "Shear Strength of Slabs," *Proceedings ASCE, Journal of the Structural Division*, vol. 100, pp. 1543–1591, Aug. 1974.

[12] A. Muttoni, "Punching Shear Strength of Reinforced Concrete Slabs without Transverse Reinforcement," *ACI Structural Journal*, vol. 105, May 2008.

[13] M. Fernández Ruiz and A. Muttoni, "Application of Critical Shear Crack Theory to Punching of Reinforced Concrete Slabs with Transverse Reinforcement," *ACI Structural Journal*, vol. 106, May 2009.

[14] G. S. M. Nivea G. B. Albuquerque and Robert L. Vollum, "Punching Shear Strength of Flat Slab-Edge Column Connections with Outward Eccentricity of Loading," *ACI Structural Journal*, vol. 113, no. 5, 2016, doi: 10.14359/51689156.

[15] N. H. and A. Ghali, "Punching Shear Resistance of Corner Slab-Column Connections," *ACI Structural Journal*, vol. 91, no. 6, 1994, doi: 10.14359/1502.

[16] N. Narayani, "Shear reinforcement in reinforced concrete column heads," Thesis Doctor of Philosophy in the Faculty of Engineering, Imperial College of Science and Technology, London, 1971.

[17] E. E.-D. R. F. Zaghlool, "Strength and behaviour of corner and edge column-slab connections in reinforced concrete flat plates (Unpublished doctoral thesis)," Doctor of Philosophy, University of Calgary, Calgary, 1971.

[18] N. N. Anis, "Shear strength of reinforced concrete flat slabs without shear reinforcement," Doctor of Philosophy, Imperial College London, London, 1970.

[19] N. W. Hanson and Hanson J. M., "Shear and Moment Transfer between Concrete Slabs and Columns," *318Reference*, vol. 11, no. 68.

[20] A. Stamenkovic, "Local strength of flat slabs at column heads," Imperial College London, London, 1970.

[21] D. Vargas, E. Lantsoght, and K. Genikomsou, "Spreadsheet for Flat slabs in eccentric punching shear: experimental database and analysis." Zenodo, Quito, 2022. doi: https://doi.org/10.5281/zenodo.6532705.

[22] M. Sarveghadi, A. H. Gandomi, H. Bolandi, and A. H. Alavi, "Development of prediction models for shear strength of SFRCB using a machine learning approach," *Neural Computing and Applications*, vol. 31, no. 7, pp. 2085–2094, Jul. 2019, doi: 10.1007/s00521-015-1997-6.

[23] Nemetschek Group, "SCIA Downloads," May 17, 2022.

[24] E. Lantsoght, "Database of Shear Experiments on Steel Fiber Reinforced Concrete Beams without Stirrups," *Materials*, vol. 12, no. 6, p. 917, Mar. 2019, doi: 10.3390/ma12060917.

[25] D. Vargas, E. Lantsoght, and K. Genikomsou, "Spreadsheet validation for Flat slabs in eccentric punching shear experimental database and analysis." Zenodo, 2022. doi: https://doi.org/10.5281/zenodo.6532745.

[26] T. Ngo, "Punching shear resistance of high-strength concrete slabs," *Electronic Journal of Structural Engineering*, vol. 1, no. 1, pp. 52–59, Jan. 2001, [Online]. Available: https://ejsei.com/EJSE/article/view/14

[27] S. Guandallini, O. L. Burdet, and A. Muttoni, "Punching Tests of Slabs with Low Reinforcement Ratios," *ACI Structural Journal*, vol. 106, pp. 87–95, 2009.